

CRC Report No. AVFL-44

**First Investigation of Ducted Fuel
Injection on a Retrofitted Heavy-Duty
Multi-Cylinder Production Engine**

Final Report

June 2025



COORDINATING RESEARCH COUNCIL, INC.
1 CONCOURSE PARKWAY • SUITE 800 • ATLANTA, GA 30328

The Coordinating Research Council, Inc. (CRC) is a non-profit corporation supported by the petroleum and automotive equipment industries with participation from other industries, companies, and governmental bodies on research programs of mutual interest. CRC operates through the committees made up of technical experts from industry and government who voluntarily participate. The five main areas of research within CRC are: air pollution (atmospheric and engineering studies); aviation fuels, lubricants, and equipment performance; heavy-duty vehicle fuels, lubricants, and equipment performance (e.g., diesel trucks); light-duty vehicle fuels, lubricants, and equipment performance (e.g., passenger cars); and sustainable mobility (e.g., decarbonization). CRC's function is to provide the mechanism for joint research conducted by industries that will help in determining the optimum combination of products. CRC's work is limited to research that is mutually beneficial to the industries involved. The final results of the research conducted by, or under the auspices of, CRC are available to the public.

LEGAL NOTICE

This report was prepared by Sandia National Laboratory as an account of work sponsored by the Coordinating Research Council (CRC). Neither the CRC, members of the CRC, Sandia National Laboratory, nor any person acting on their behalf: (1) makes any warranty, express or implied, with respect to the use of any information, apparatus, method, or process disclosed in this report, or (2) assumes any liabilities with respect to use of, inability to use, or damages resulting from the use or inability to use, any information, apparatus, method, or process disclosed in this report. In formulating and approving reports, the appropriate committee of the Coordinating Research Council, Inc. has not investigated or considered patents which may apply to the subject matter. Prospective users of the report are responsible for protecting themselves against liability for infringement of patents.

First investigation of ducted fuel injection on a retrofitted heavy-duty multi-cylinder production engine

Ryan M. Ogren¹, Kirby J. Baumgard², Vishnu Radhakrishna³, Robert C. Kempin³,
and Charles J. Mueller³

¹John Deere, ²Baumgard Technologies, ³Sandia National Laboratories

ABSTRACT

Ducted fuel injection (DFI) was tested for the first time on a production multi-cylinder engine using a John Deere Model 6090 heavy-duty diesel engine. Design-of-experiments (DoE) testing was carried out for DFI with a baseline ultra-low sulfur diesel (ULSD) fuel as well as three fuels with lower lifecycle carbon-dioxide (CO₂) emissions: renewable diesel, neat biodiesel (from soy), and a 50/50 blend by volume of biodiesel with renewable diesel. For all fuels tested, DFI enabled simultaneous reductions of engine-out emissions of soot and nitrogen oxides (NO_x) with late injection timings. DoE data were used to develop individual calibrations for steady-state testing with each fuel using the ISO 8178 eight-mode off-road test cycle. Over the ISO 8178 test, DFI with a 5-duct configuration and B50R50 fuel reduced soot and NO_x by 87% and 42%, respectively, relative to the production hardware. Soot reductions generally decreased with increasing engine load. Hydrocarbon and carbon monoxide emissions tended to increase with DFI but were not excessive over the ISO 8178 test. Brake-specific energy consumption generally increased with DFI due to the use of retarded injection timings and exhaust-gas recirculation to achieve the desired NO_x reductions but was less than or equal to that for conventional diesel combustion with ULSD at a similar NO_x level. Significant deposits were encountered on one cylinder when running at idle with the ULSD fuel only, but this was mitigated by replacing the corresponding fuel injector (which showed deformation at the exits of two of its orifices) and using a fuel detergent additive in subsequent testing. In all, the engine was successfully operated for over 300 hours in the DFI configuration. Research areas for improved DFI implementation are identified.

INTRODUCTION

Established refueling infrastructure, high energy density, and high efficiency of compression-ignition engines are predicted to support continuous demand for diesel fuels through 2050 [1]. Nevertheless, diesel engine manufacturers will be required to meet increasingly stringent emissions mandates while minimizing expense to the end user. Perhaps the largest challenge in this regard is simultaneously reducing nitrogen oxides (NO_x) and particulate matter (PM) without increasing initial or operating costs or sacrificing reliability/durability.

Current state-of-the-art diesel power plants leverage selective catalytic reduction (SCR) with diesel exhaust fluid (DEF) to reduce engine-out NO_x to regulated limits. A diesel particulate filter (DPF)

traps engine-out PM while an ammonia slip catalyst treats for any remaining ammonia from the SCR [2]. For the same engine-out emissions aftertreatment system (ATS) size, the flow restriction and total cost of ownership will likely increase with more-stringent NOx and soot regulations. Strong demand exists for a low-cost technology that can reduce engine-out emissions (and therefore ATS cost) and total fluid consumption (DEF + fuel).

Ducted fuel injection (DFI) is a technology that enables simultaneous reductions in engine-out soot and NOx. Invented at the Combustion Research Facility at Sandia National Laboratories, DFI utilizes small ducts aligned to each injector orifice to enhance air entrainment into the fuel spray and subsequent mixing prior to autoignition [3]. Figure 1 shows a 4-duct DFI module installed on a John Deere diesel engine. DFI reduces soot at least in part by decreasing the equivalence ratio at the flame liftoff length. Fuel entering the duct creates an area of low-pressure where a jet-pumping effect entrains more air than a free spray [4,5]. Inside the duct, steep velocity gradients drive enhanced turbulent mixing [4,6]. If the spray flame is lifted from the duct exit, secondary air-entrainment and mixing can occur, further lowering soot production [7,8].



Figure 1. 4H DFI installed on a John Deere multi-cylinder diesel engine.

A schematic of the geometry of a DFI duct is shown in Figure 2. Gehmlich and co-authors examined duct geometry in a constant-volume combustion vessel using a 0.09-mm orifice injector and nominal ambient density of 22.8 kg/m³. Rounding the inlet and tapering the exit (δ -configuration) improved DFI soot reduction. Soot was insensitive to standoff distance (G) for values below 4 mm and increased as the duct was moved farther away from the orifice. Gehmlich established a duct naming convention that will be used in this paper and is as follows: D {diameter} L {length} G {standoff distance} {inlet/outlet configuration} where D , L , and G are shown in Figure 2 in the δ configuration [7].

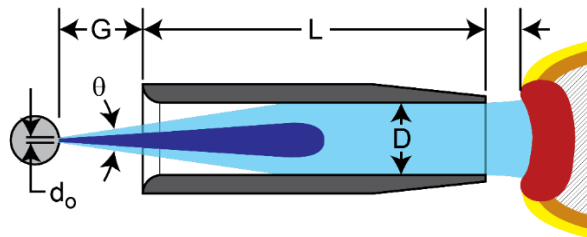


Figure 2. Schematic showing DFI parameters.

Nilsen and colleagues were the first to examine the impact of duct geometry on-engine using a 0.175-mm injector orifice at 13.4 bar gross indicated mean effective pressure (IMEP_g). Soot was minimized using a D3L12G3 δ configuration, indicating that a cross-sectional area ratio (duct to orifice) of 300 may be optimal [9]. Later work from Svensson et al., using a 0.15-mm injector orifice, recommended a smaller ratio of 180-220 [10].

The alignment of each duct to the injector orifice is critical to the efficacy of DFI in reducing PM [3,7]. A recent study found that for optimum performance the duct axis should be within 0.125 mm of the injector spray centerline [11].

Caterpillar installed a 6-duct DFI module with a D2.5L14G3.8 δ configuration on a heavy-duty single-cylinder engine and carried out limited parameter sweeps at high load at 1000 and 1800 RPM. The study reported soot increases with DFI relative to conventional diesel combustion (CDC) for a BSNO_x range of 4-8 g/kWh with exhaust-gas recirculation (EGR). Filter smoke number generally decreased with NO_x, indicating that if timing had been further retarded, filter smoke number may have been reduced relative to CDC [12].

Piano and colleagues used CFD to model a light-duty diesel engine retrofitted with DFI. They found that DFI reduces soot formation but that the duct assembly itself can limit late-stage mixing relative to CDC. The increased liftoff length of DFI created fuel-rich zones at the bowl wall which the authors suggested may scale with bore size [13]. An optical-engine study by Pastor and colleagues confirmed a reduction in soot formation and loss of soot oxidation using two-color pyrometry with DFI retrofit to a medium-duty engine. In contrast to a free-spray, chemiluminescence and two-color pyrometry mapping showed evidence of reduced mixing nearer to the injector over the combustion cycle with DFI [14]. Both Pastor and Piano emphasized the need for calibration and hardware optimization for DFI.

Current Study

The primary objective of the current study was to achieve the first successful implementation of DFI in a multi-cylinder, near-production, heavy-duty diesel engine. In this case, “successful” is defined as achieving ~70% lower engine-out soot and lifecycle-CO₂ emissions, simultaneously with ~50% lower engine-out NO_x emissions, and without large adverse effects on engine-out hydrocarbon (HC) or carbon monoxide (CO) emissions or brake-specific energy consumption (BSEC, defined as the ratio of chemical energy input to brake work output). The baseline for determining the improvements is a state-of-the-art, production CDC engine without aftertreatment, operated with petroleum diesel fuel over the industry-standard ISO 8178-C1 off-road steady-state test cycle. As shown below in Figure 15 and corresponding discussion, this objective was achieved.

The structure of the paper is as follows. The Materials and Methods section describes the fabrication, installation, and alignment of the DFI components with the John Deere cylinder head and fuel injectors, as well as how the John Deere DFI engine was calibrated via DoE testing for the ISO 8178 modes running both ULSD and low-lifecycle-CO₂ fuels (LLCFs). The Results and Discussion section presents the DoE and ISO 8178 results for DFI four- and five-duct configurations with ULSD and the LLCFs relative to the Tier 4 Final (T4F) production CDC hardware with ULSD, including discussion of an isolated event at the start of the test campaign during which one of the six duct modules became plugged with deposits. The paper ends with the Summary and Conclusions section listing the primary findings of the study.

MATERIALS AND METHODS

Duct Installation and Alignment

Alignment of each diesel spray to its corresponding duct is critical for achieving optimal DFI performance [3,7,11] and was carefully addressed in this study. The installation employed required fabrication of a duct module and a flange bolt for each cylinder, as shown in Figure 3. Machining of the cylinder head was also required. The diameter of the lower section of each injector bore through which the injector tip passes was increased to allow its flange bolt to fit through the bore and screw into its duct module. Each duct module has a tang machined into its base that fits into a mating pocket machined into the cylinder head. This design allowed for fine duct rotational-alignment adjustments using shims of different thicknesses on either side of the tang. The desired vertical alignment was established by grinding the top of the flange bolt to the appropriate thickness. To facilitate combustion gas sealing, a 0.13-mm-thick graphite foil gasket was placed between each flange bolt and its injector.

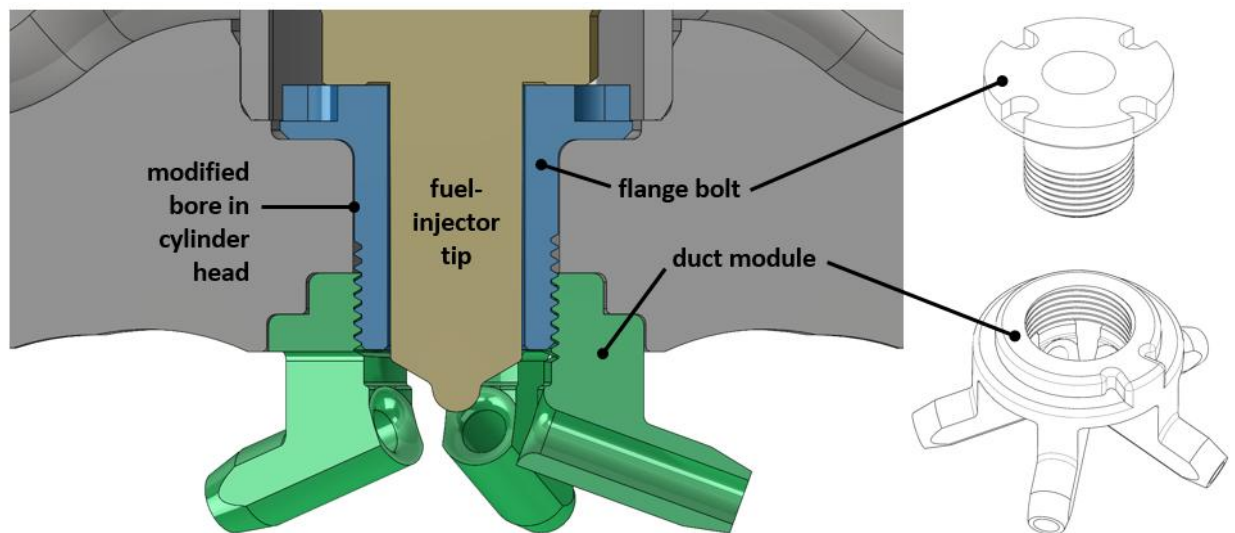


Figure 3. Installation of the duct module onto the engine cylinder head.

Duct alignment was verified by placing a polycarbonate plastic plug into each duct and using a portable fuel-injection system to fire each cylinder individually with the head on a test bench. The portable fuel-injection system included a high-pressure hand pump, 5- μm filter assembly, mechanical pressure gauge, high-pressure line, and injector-driver electronics. The injection pressure employed was 180 MPa, and typically two injections of approximately 2 ms each were fired to obtain a sufficient witness mark on each alignment plug. The marked plugs were then removed from the duct module and placed in a holder that attached to a transverse microscope table to allow images to be taken of each witness mark (see Figure 4). The images were processed using MATLAB to determine the x- and y-offsets between the center of each plug and its corresponding witness mark. In the processing stage, three points were manually selected along the outer edge of the plug to define its circular boundary, allowing for the calculation of its center coordinates. Similarly, three points were selected along the outer edge of each circular witness mark to determine its boundary and compute its center coordinates. Next, the x- and y-offsets were obtained by calculating the difference between the center coordinates of the plug and its witness mark. These offset measurements were then used to determine any required adjustments in the rotational shim thicknesses (x-offset) and the flange-bolt flange thickness (y-offset). Measurements taken after the final 4-duct alignment showed the averaged rotational offset was 0.027 mm with a two-standard-deviation (2σ) interval of 0.192 mm, and the vertical offset was $0.031 \text{ mm} \pm 0.091 \text{ mm}$ (2σ).

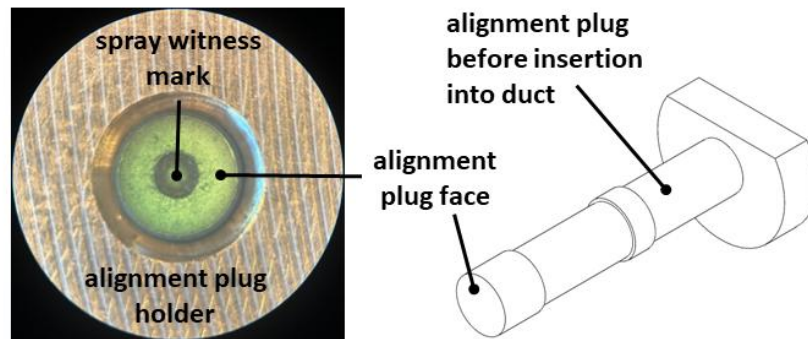


Figure 4. Polycarbonate alignment plug and witness mark showing good spray/duct alignment.

With some exceptions, the cylinder head was removed after testing a given fuel and DFI configuration; the ducts were inspected and cleaned if necessary to remove any thin film of carbon on the inside of the ducts (only required during 4-duct testing), and the alignment was checked. It was hypothesized that the spray/duct alignment did not change during operation and that the variability in the offset measurements from one set of tests to the next was dominated by measurement variability and possibly changes in the fuel spray pattern. This hypothesis was supported by noting the scatter in offset measurements acquired during repeated alignment tests with the head on the test bench and without any alignment adjustments between repeats.

The alignment procedure was changed before testing with the 5-duct modules. The main reason for the change was to improve the centering of the injector nozzle in the duct module. Several potential causes of the observed non-concentricity were:

1. The upper bore in the cylinder head for the injector body was not concentric with the lower bore for the injector nozzle.
2. Installation of the injector side-feed tube forced the injector to one side of the upper injector bore (see Figure 5).
3. Due to fuel-injector assembly tolerances, the injector nozzle tip was not perfectly coaxial with the injector body.

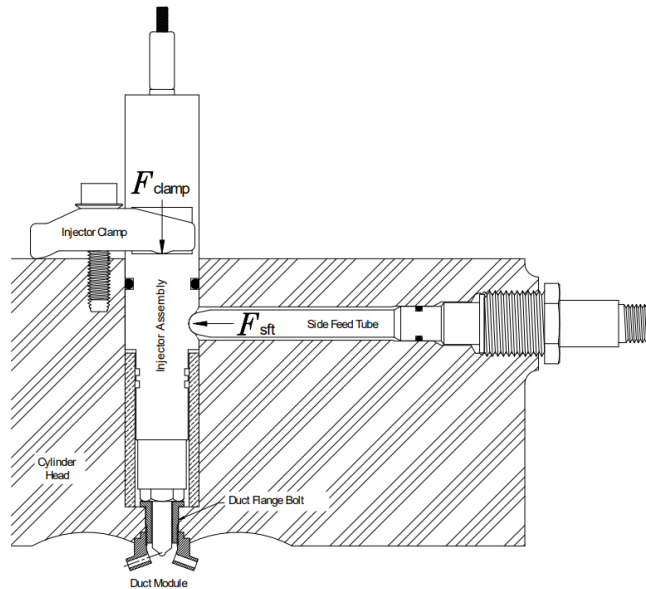


Figure 5. Clamping and side-feed tube forces on the installed injector.

Using measurements of runout between the upper and lower injector bores and between the injector bodies and nozzles, it was decided to machine a 0.18-mm offset in the upper injector bore. This allowed shims to be placed opposite the side-feed tube and 90° from the side-feed tube to establish the desired concentricity between the injector and the duct module. Injector nozzle-tip alignment was verified by using a 0.076-mm feeler gauge and verifying clearance between the nozzle tip and the inner wall of the flange bolt. Once all six injectors were installed and checked with the feeler gauge, final alignment was verified by firing into the polycarbonate plugs and measuring the offsets of the witness marks. Figure 6 shows the offsets for all six cylinders. The average offset of all 30 witness marks was 0.005 ± 0.057 mm (2σ) in the rotational direction and 0.011 ± 0.051 mm (2σ) in the vertical direction, a significant improvement over the 4-duct alignment.

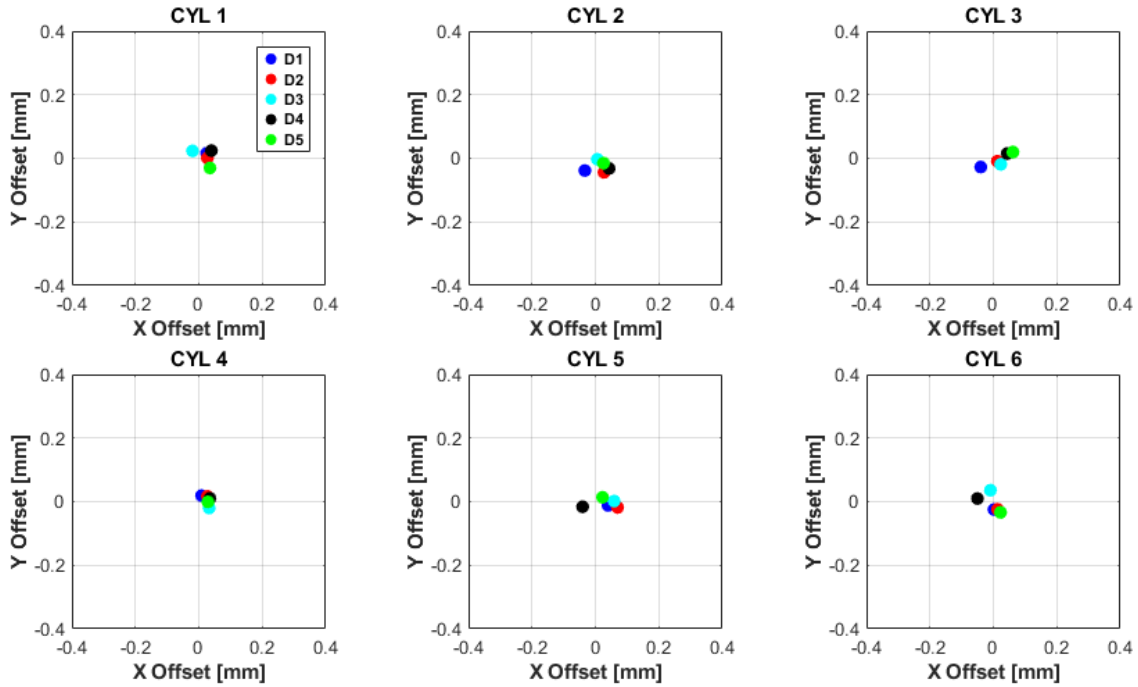


Figure 6. Offset measurements for all six cylinders using the 5-duct modules.

Engine and Test-Cell Setup

Details regarding the John Deere multi-cylinder engine can be found below in Table 1. Fuel-injector orifice diameters were adjusted with the number of orifices to maintain a constant steady flow through the injector. Hence, the 7-hole (7H) CDC injector had smaller orifices than the 4-hole (4H) and 5-hole (5H) DFI injectors. The John Deere engine control unit was used to command injection timing/quantity, injection pressure, actuator positions for air-fuel ratio, and EGR. The production-piston apex was machined down 2 mm to accommodate the duct module in the combustion chamber.

Test-cell details can be found in Table 2. EGR was monitored by measuring intake manifold CO₂ content. Cylinder pressure data were captured to verify similar IMEP_g across cylinders. No ATS was used and only engine-out emissions were measured. An exhaust restriction butterfly valve was applied to mimic ATS backpressure. All engine testing was carried out at Excel Engineering in Diagonal, Iowa.

Table 1. John Deere 6090 Engine Details

Engine	6090RX501
Compression Ratio/Number of Cylinders	15.9/6
Bore/Stroke [mm]	118/136
Engine Oil	15W-40
Air System	Dual-stage turbocharging with variable turbocharger geometry, EGR-valve, and air-throttle
Fuel System	Denso high-pressure common rail

7H CDC Production Injector	Denso 7 x 0.175 mm x 133° G4 solenoid
4H DFI Injector	Denso 4 x 0.232 mm x 140° G4 solenoid
5H DFI Injector	Denso 5 x 0.208 mm x 140° G4 solenoid
DFI Modules	D2.5L12G3δ

Table 2. Test Cell Equipment

Dynamometer	Baldor Reliance AC motor with Mitsubishi FR-A842-10940-1-UR controller
Torque Measurement	HBM T40B torque flange
Emissions Bench	Horiba Mexa-7100DEGR
EGR	CO ₂ sample probe at center of intake manifold
PM Sampling	Sierra BG3 with partial flow dilution system
Smoke Measurement	AVL 415 Smoke Meter
Soot measurement	AVL 483 Micro-Soot Sensor
Combustion Air Flow	Meriam Z50MC2-6 laminar flow element
Fuel Flow	Custom Excel Engineering gravimetric flow meter with density correction
Data Acquisition	Cyflex™ system
High-Speed Data Acquisition	Six ea. Kistler 6052 transducers with AVL Indicom system

Test Procedure

Design-of-experiments (DoE) testing was carried out for each combustion-strategy/test-fuel combination at each of the ISO 8178 modal conditions listed in Table 3. Boundary conditions detailed in Table 4 were set and locked at the rated-power/Mode-1 (M1) condition. DoE testing manipulated injection timing, rail pressure, and air-system actuator positions for EGR flow and air-fuel ratio. DoE results at each mode were modeled in ETAS ASCMO software.

Testing commenced with the collection of reference data with CDC production hardware (Table 1) and T4F engine-out NO_x calibration levels (High-NO_x or HN) using ULSD as fuel. Next, the production calibration was modified through DoEs to achieve ~50% NO_x reduction (Low-NO_x or LN) using increased EGR, curtailed air flow, timing retard, and/or lower injection pressure with ULSD. The LN CDC calibration was not optimized but is considered a general reference point. ISO 8178-C1 testing was carried out for both the HN and the LN CDC calibration with ULSD.

DoE data were then acquired in a similar manner for each DFI configuration with each test fuel, and these data were used to create a distinct LN calibration for each configuration and fuel that minimized soot at 50% of the production T4F engine-out NO_x level. BSEC was not included in the optimization that was employed to select the DoE test points. BSEC is used rather than brake-

specific fuel consumption because the fuels have different lower heating values, as shown in Table 5.

Although BSEC minimization was not a part of the optimization process for generation of the LN calibration (i.e., selection of the DoE test points), it was used to select the “optimal” DFI points shown in the DoE figures below by minimizing the following cost function:

$$C_{i,j} = \frac{NOx_{i,j} - 0.3NOx_{HN,j}}{0.3NOx_{HN,j}} \mathcal{H}(NOx_{i,j} - 0.3NOx_{HN,j}) + \frac{soot_{i,j} - 0.3soot_{HN,j}}{0.3soot_{HN,j}} \mathcal{H}(soot_{i,j} - 0.3soot_{HN,j}) + [BSEC_{i,j} - (BSEC_{HN,j} - 1.5)] \mathcal{H}[BSEC_{i,j} - (BSEC_{HN,j} - 1.5)] \quad (1)$$

where i indicates a given test-point in the DoE, j the given mode number, and \mathcal{H} the Heaviside step function. The cost function in Eq. 1 decreases for NOx and soot reductions up to but not beyond 70% and BSEC values up to the T4F level at the given mode minus 1.5, the latter of which will give credit for effectively all realistic BSEC reductions.

Emissions checkpoint and cylinder cut-out tests were carried out daily at the M3 condition. These tests verified the consistency of measurements and the cylinder-to-cylinder variation in IMEP_g levels.

Table 3. 277 KW ISO 8178-C1 Steady-State Test Modes

ISO 8178-C1 Mode	Composite Score Weight	Engine Speed [RPM]	Engine Torque [NM]	Fuel Injection Strategy
1	0.15	2100	1267	Single Inject
2	0.15	2100	950	Single Inject
3	0.15	2100	633	Single Inject
4	0.1	2100	127	Pilot-Main-Post
5	0.1	1575	1789	Single Inject
6	0.1	1575	1342	Single Inject
7	0.1	1575	894	Single Inject
8	0.15	800	50	Pilot-Main

Table 4. DoE and ISO 8178-C1 Boundary Conditions

Boundary Condition	Setpoint	Additional Detail
Combustion Air Temperature [°C]	25 ± 5	Maintained for all conditions
Combustion Air Dew Point [°C]	9 ± 1	
Fuel Inlet Temperature [°C]	40 ± 5	
Coolant Outlet Temperature [°C]	98 ± 2	
Intercooler Outlet Temperature [°C]	52 ± 2	Set at M1 condition
Intake Restriction [kPa]	3 ± 1	

Intercooler Restriction [kPa]	16 ± 1
Exhaust Back-Pressure [kPa]	23 ± 1

Table 5. Test Fuel Lower Heating Values

Test Fuel	Lower Heating Value, LHV [MJ/kg]
Ultra-Low-Sulfur Diesel #2 (ULSD)	42.87
Renewable Diesel (R99)	43.97
B100	37.4
B50R50	40.69

RESULTS AND DISCUSSION

The major findings of this study are presented in the following six sections. The first section shows results from the DoE testing at the ISO 8178 modal points for DFI with the 5-hole (5H) injector for the B50R50 and RD fuels vs. CDC with the 7-hole (7H) injector and ULSD fuel. These data were used to select the DFI 5H operating points for the ISO 8178 test cycle for RD and B50R50, the results of which are shown in the second section. The third section compares CDC to DFI with the same fuel (RD), enabling DFI effects to be separated from fuel effects. The fourth section compares DFI 5H vs. 4H performance for the B50R50 and RD fuels. The fifth section covers the effects of ULSD, RD, B50R50, and B100 on performance with the DFI 4H configuration. The sixth section discusses a duct-fouling event that occurred at the beginning of the test campaign, the steps that were taken to mitigate subsequent fouling, and the investigation into the root cause of the fouling.

Design-of-Experiments (DoE) Testing

For brevity and simplicity, the following discussion focuses on results for B50R50 fuel because it is likely to have the largest benefit in terms of lifecycle-CO₂ emissions while still being feasible for general use. Results for the M1, M3, M5, and M7 conditions are shown because they bracket the speed/load range where most fuel is consumed in most applications. Results are also presented for M8 to give a sense of DFI performance at light-load conditions. For completeness, the M2, M4, and M6 data for DFI 5H B50R50 are given in the Appendix as Figures A1-A3, respectively, and Figure A4 shows soot/NO_x tradeoff plots for all the modes. The DoE data for M1-M8 with DFI 5H RD can be found in Figures A5-A12, respectively, and Figure A13 shows the corresponding soot/NO_x tradeoff plots. Single injections were used for most operating conditions. While M4 and M8 employed multiple injections, pilot- and post-injection quantity/timing sweeps were not widely explored.

Figure 7 shows results from DoE testing at M1 of the ISO 8178-C1 test cycle. M1 is the full-load, rated-speed (i.e., rated-power) condition. Data for two combustion-strategy/fuel conditions are presented: the stars show CDC 7H ULSD data, while the circles show DFI 5H B50R50 data. The left and center plots show engine-out soot and NO_x, respectively, normalized by the corresponding baseline values, vs. the actual start of injection timing (SOI) shifted by the baseline SOI. Hence, a positive value of the shifted SOI corresponds to a timing retard relative to baseline. The right plot shows the change in BSEC relative to the baseline. The baseline data point in each plot is indicated by the red-outlined star. The red-outlined circle in each plot shows the optimal DFI point. Each point is colored according to its percentage change in EGR relative to the baseline (i.e., not an absolute change in %EGR), as indicated by the color bar on the far right. Independent variables in addition to SOI and EGR level changed in the DoE testing, including injection pressure and air/fuel ratio. Nevertheless, changes in SOI and EGR level seem to capture most of the first-order effects on emissions and BSEC.

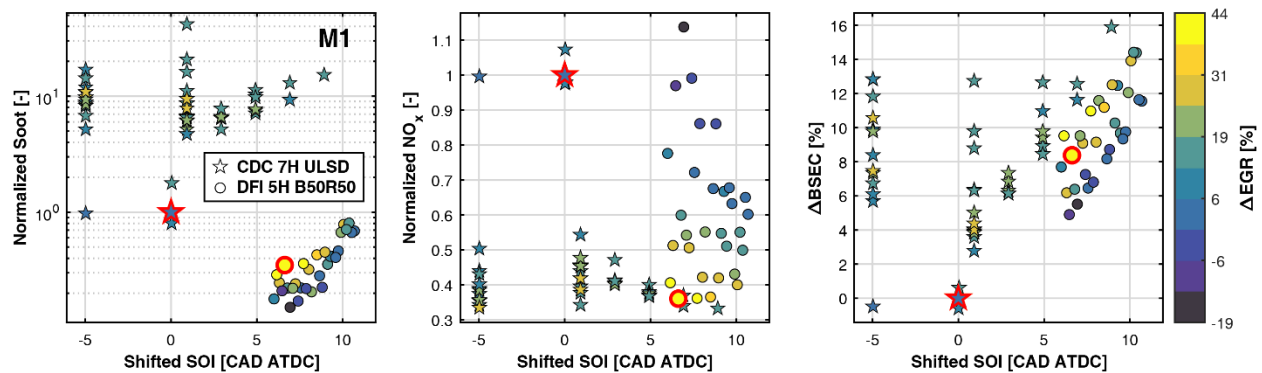


Figure 7. DoE data showing normalized engine-out soot and NO_x as well as ΔBSEC vs. shifted SOI timing and relative change in EGR level for CDC 7H ULSD vs. DFI 5H B50R50 at M1 (100% speed, 100% load) of the ISO 8178 test cycle.

Figure 7 shows that at M1, the optimal DFI 5H B50R50 point reduces soot by 65% and NO_x by 64%, but it increases BSEC by 8.4%. The left plot shows that soot increases strongly as timing is retarded for both CDC and DFI, but for a given SOI timing, the soot emissions for DFI are more than an order of magnitude lower than those for CDC. It is evident that the optimal SOI timing for DFI is retarded from baseline by 6.6 CAD, which likely helps to explain the NO_x decrease as well as the BSEC increase for DFI. The center plot shows that retarding timing and increasing EGR are effective NO_x-reduction techniques for both CDC and DFI, but higher levels of EGR may be desirable for DFI. The plot on the right shows that increasing timing retard causes BSEC to increase regardless of the combustion strategy, and adding EGR tends to amplify the BSEC increase. It appears that an earlier SOI coupled with high EGR could lead to a smaller BSEC penalty for this mode. For the same SOI retard of ~7 CAD from the baseline timing, the BSEC penalty for CDC is ~12%, whereas for DFI it may only be 5-6% (depending on EGR level).

M1 heat-release-rate and cylinder pressure plots from the ISO 8178 tests are shown in Figure 8. The peak heat release rate is ~10% higher for both DFI cases but phased later from baseline CDC.

Increases in peak heat-release rate at a given mode correlate with soot reduction relative to CDC. With the exception of M5, the other single-injection modal points show differences between CDC and DFI that are similar to those observed at M1. (The analogous plot for M5 is shown in Figure 11.)

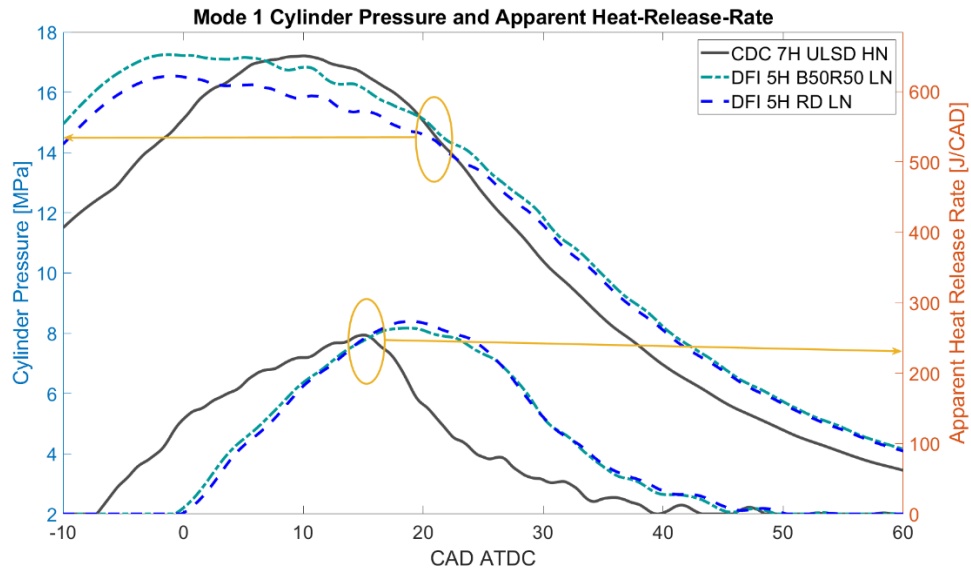


Figure 8. M1 cylinder pressure and apparent-heat-release-rate (right) for CDC vs DFI

Figure 9 shows the performance at M3, the full-speed, 50%-load condition. The optimal DFI 5H B50R50 point reduces soot by 88% and NO_x by 59%, but it increases BSEC by nearly 11%. Again, soot levels are more than an order of magnitude lower for DFI than CDC at the same SOI timing. Unlike for M1, at this mode retarding the injection timing generally leads to a soot reduction for DFI, but it again appears possible that advancing the timing while maintaining high EGR could mitigate the BSEC penalty without large increases in soot or NO_x.

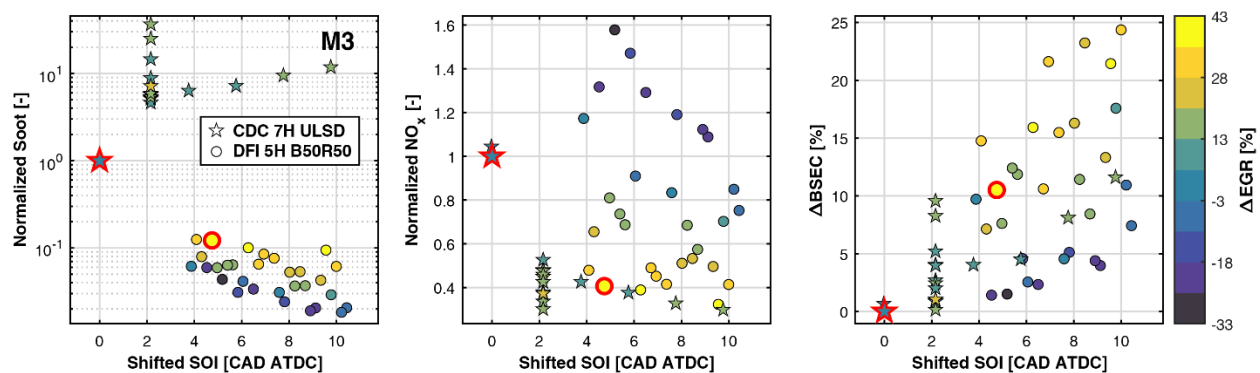


Figure 9. DoE data showing normalized engine-out soot and NO_x as well as ΔBSEC vs. shifted SOI timing and relative change in EGR level for CDC 7H ULSD vs. DFI 5H B50R50 at M3 (100% speed, 50% load) of the ISO 8178 test cycle.

Figure 10 shows the performance at M5—100% load at 75% speed—which roughly corresponds to the peak-torque point of the engine. The baseline soot emissions are near the detection limit of the AVL Micro-Soot Sensor at this condition, making the achievement of further emissions reductions particularly challenging. Nevertheless, the optimal DFI 5H B50R50 point reduces soot by 45% and NO_x by 24%, and it increases BSEC by only 3.0%. The lower BSEC penalty for DFI at M5 seems to make sense because the timing retard and EGR increase for DFI are smaller at this mode than at others.

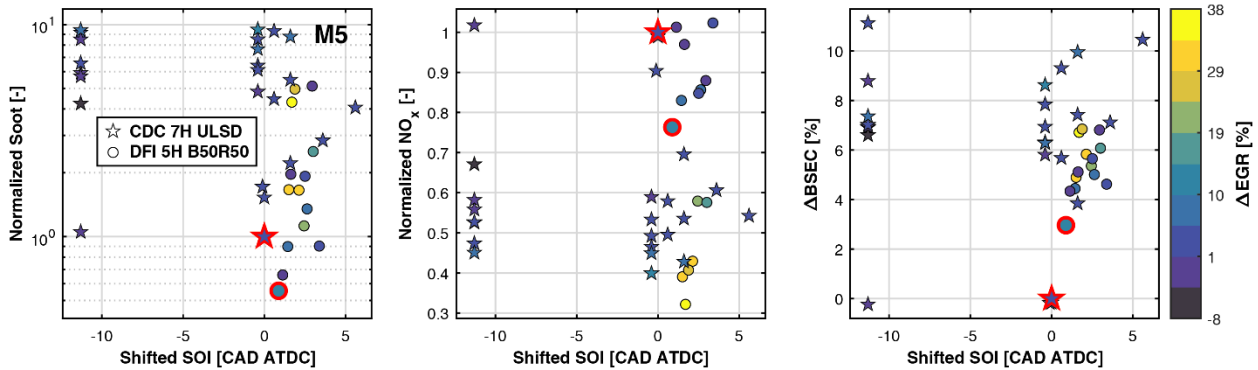


Figure 10. DoE data showing normalized engine-out soot and NO_x as well as ΔBSEC vs. shifted SOI timing and relative change in EGR level for CDC 7H ULSD vs. DFI 5H B50R50 at M5 (75% speed, 100% load) of the ISO 8178 test cycle.

M5 heat-release rate and cylinder-pressure plots from the ISO 8178 tests are shown in Figure 11. Like M1, DFI combustion is phased later than CDC but, uniquely, to a lesser extent due to the enforcement of an exhaust-temperature limit. The peak heat-release rate of DFI is 5-10% lower than that of CDC.

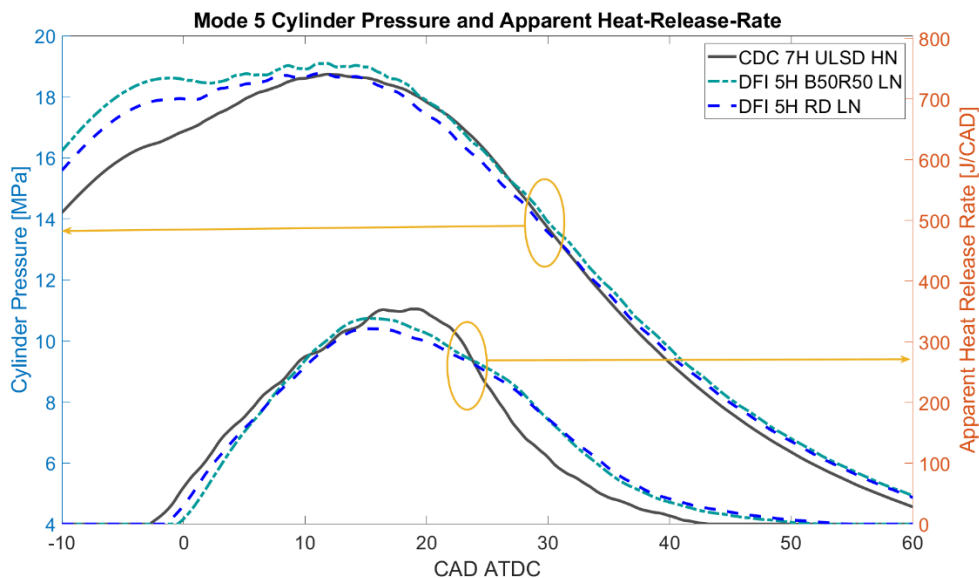


Figure 11. M5 cylinder pressure and apparent-heat-release-rate (right) for CDC vs DFI

Figure 12 shows the performance at M7, which corresponds to 50% load at 75% speed. The optimal DFI 5H B50R50 point reduces soot by 75% and NO_x by 62%, but it increases BSEC by 4.9%. The observed trends are similar to those for M1 and M3, but interestingly, the DFI requirement for timing retard at this mode appears to be driven more by soot control than NO_x control, because low-NO_x operation is possible at less-retarded timings and higher EGR.

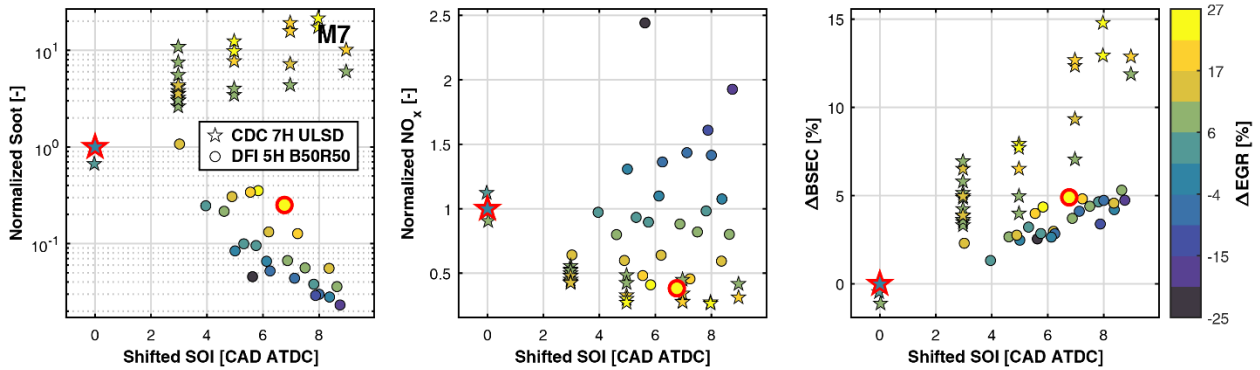


Figure 12. DoE data showing normalized engine-out soot and NO_x as well as ΔBSEC vs. shifted SOI timing and relative change in EGR level for CDC 7H ULSD vs. DFI 5H B50R50 at M7 (75% speed, 50% load) of the ISO 8178 test cycle.

Figure 13 shows the performance at M8, which corresponds to idle. Soot reductions of more than two orders of magnitude are possible with DFI at this mode, which employs a pilot-main injection strategy. The optimal DFI 5H B50R50 point reduces soot by 98% and NO_x by 69%. In contrast to the other modes discussed above, BSEC *decreases* by 13% for DFI rather than increasing, despite the introduction of EGR at this condition and a 1.4 CAD SOI main-injection timing retard. DFI performs quite well at M8 in terms of both emissions and BSEC.

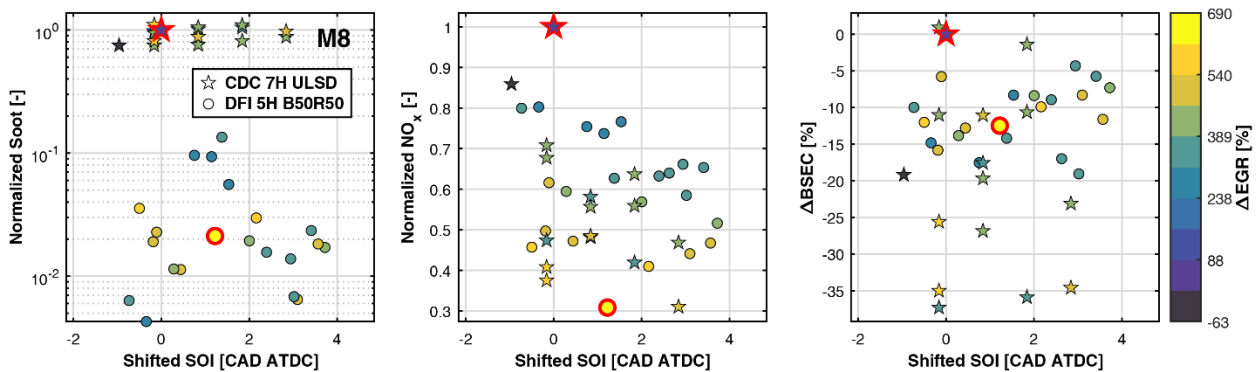


Figure 13. DoE data showing normalized engine-out soot and NO_x as well as ΔBSEC vs. shifted SOI timing and relative change in EGR level for CDC 7H ULSD vs. DFI 5H B50R50 at M8 (idle) of the ISO 8178 test cycle.

Full-Cycle ISO 8178 Testing Using Final Calibrations

A “best” operating point was determined based on the DoE testing of each DFI configuration at each mode with each fuel, and the set of modal best points became the final calibration for that DFI configuration and fuel. The engine was then operated over the full ISO 8178 test cycle using

each final calibration to estimate the potential performance impacts of changing the DFI configuration and fuel.

Injection timing retard for DFI on the ISO 8178-C1 test relative to the T4F calibration is shown in Figure 14. Modes 4 and 8 used multiple injections and show less main-timing retard relative to the T4F calibration. For the CDC LN calibration no retard was applied at M8. While the DFI LN calibrations generally use late timings to minimize both NOx and soot, the CDC LN calibration leverages late timings to minimize NOx only. The exhaust-temperature limitation restricted the extent of timing retard at M5.

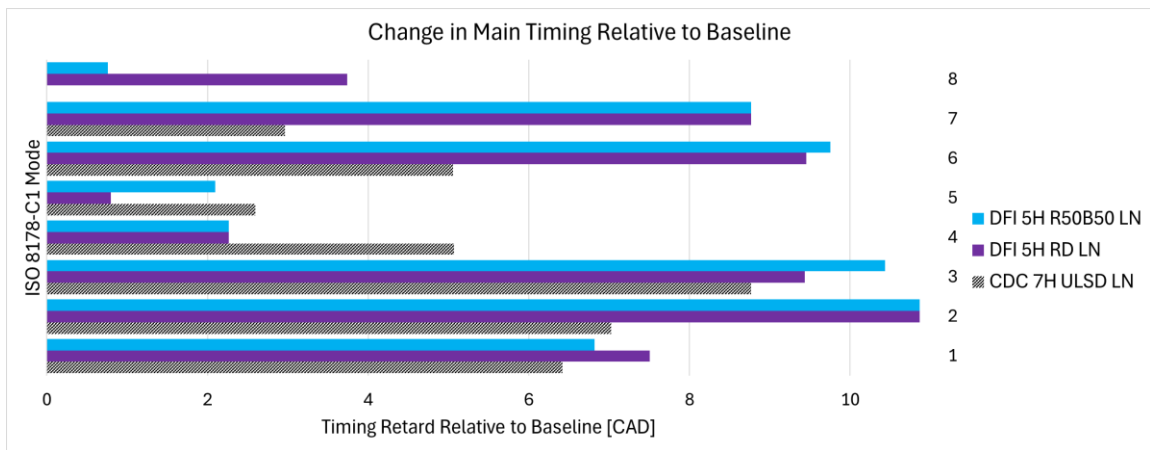


Figure 14. Timing retard relative to baseline at each modal point to achieve 50% NOx reduction while minimizing soot for DFI.

The next step was to run full-cycle ISO 8178 tests using the final calibrations for each DFI configuration and fuel, and compare the results to the baseline CDC calibration. For this subsection, the baseline calibration is CDC 7H ULSD HN, which is compared to the following LN calibrations: CDC 7H ULSD, DFI 5H RD, and DFI 5H B50R50. Figure 15 provides the results from an average of at least two composite ISO 8178-C1 tests for each DFI case, where the values shown are the changes relative to the baseline performance.

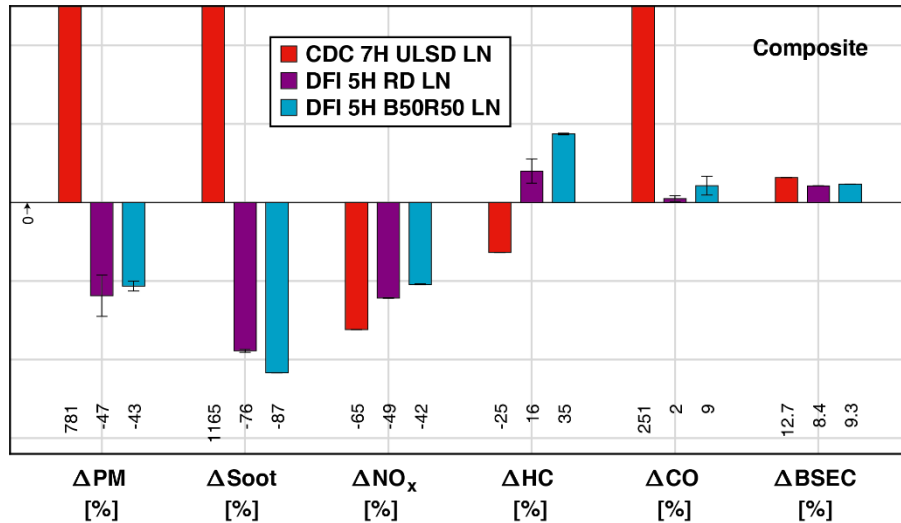


Figure 15. ISO 8178 composite results for CDC and DFI 5H low-NO_x (LN) calibrations. The baseline used for calculating changes is CDC 7H ULSD HN, i.e., the Tier 4 Final engine calibration.

Figure 15 offers valuable insights into the performance of DFI vs. CDC. It shows that attempting to achieve a large NO_x reduction using the CDC 7H ULSD configuration through a combination of timing retard and increased EGR leads to huge increases in PM, soot, and (to a lesser extent) CO, as well as an increase in BSEC. It also shows that using the DFI 5H configuration with RD or B50R50 gives substantial reductions of both PM and soot at comparable NO_x and with a smaller BSEC penalty than the CDC LN calibration. HC and CO emissions increase with DFI but do not exceed a 35% increase relative to CDC composite scores. The RD and B50R50 fuels inherently provide an ~70% reduction in lifecycle-CO₂ emissions, their soot reductions have surpassed the 70% goal set forth in the project, and the ~50% NO_x-reduction target also has been achieved. This is noteworthy given that this is the first DFI testing in an MCE, and it uses a combustion-chamber design optimized for CDC rather than DFI. It is also worth mentioning that RD and B50R50 perform quite similarly, with RD offering a 7% larger NO_x reduction but an 11% smaller soot attenuation than B50R50. Finally, the DFI gravimetric PM reductions are not as large as the soot (i.e., black carbon) reductions. This is due to an increased volatile fraction for DFI PM, which should be effectively removed by the oxidation catalyst already present on effectively all modern diesel engines [15-18].

While for brevity only composite results from ISO 8178 testing are presented above and in the rest of the main body of this paper, results for individual modes are provided in the Appendix in Figures A14-A21.

CDC vs. DFI with RD

The results in Figure 15 show the combined effects of changing the combustion strategy from CDC 7H to DFI 5H and changing the fuel from ULSD to RD and B50R50. Apparently, the increase in soot expected from using the larger orifices of the 5H nozzle is more than offset by switching to

DFI and the LLCFs. Given that ULSD contains aromatic compounds that are known to promote soot formation [19,20] while RD and B50R50 do not, one might wonder whether the PM and soot benefits observed in Figure 15 might be more due to the change in fuels rather than the change in combustion strategy. Although large soot reductions with DFI for the same fuel and same injector configuration have been reported previously [21-23] and this was not a primary focus of the current study, Figure 16 addresses this question. The baseline for Figure 16 is now CDC 7H RD HN, so the reductions in this plot are all for the same RD fuel.

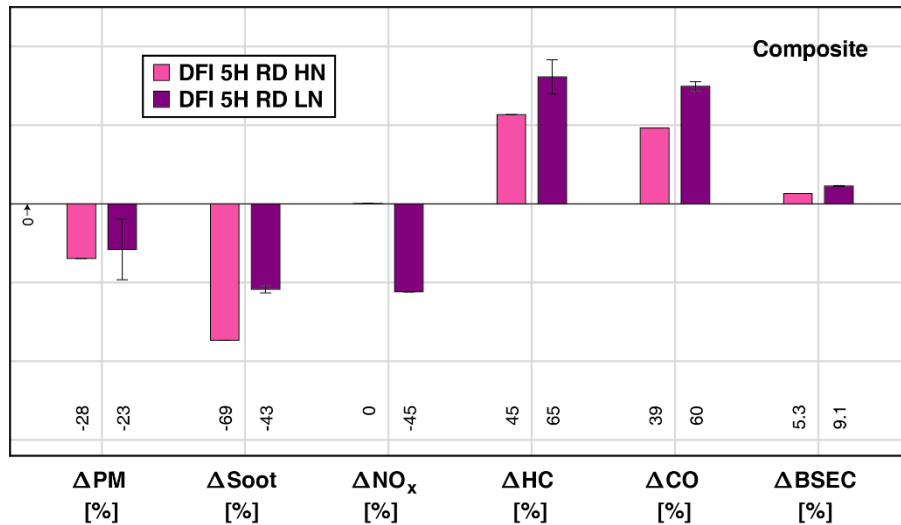


Figure 16. ISO 8178 composite results for DFI 5H RD high-NO_x (HN) and low-NO_x (LN) calibrations. The baseline used for calculating changes is CDC 7H RD HN with the Tier 4 Final engine calibration.

Figure 16 shows that switching from CDC 7H to DFI 5H at the HN calibration while using the same RD fuel (pink bars) leads to 69% lower soot and 28% lower PM at constant NO_x, reinforcing the substantial benefit provided by DFI. Notably, this benefit is achieved even though the CDC 7H injector orifices are smaller and hence less prone to soot formation than the DFI 5H injectors, which have the same steady flow. HC and CO emissions are higher than baseline largely due to increases at M4 and M8 (see Figures A17 and A21). The BSEC penalty with DFI is smaller than shown in Figure 15, likely because the required timing retard and EGR levels are lower due to the NO_x target being higher. Nevertheless, DFI still shows a 5.3% BSEC increase relative to CDC, and further investigation is required to determine the root cause. When moving from the DFI HN to LN calibration, some of the DFI soot, HC, CO, and BSEC performance are traded off for lower NO_x (purple bars).

DFI Performance Comparison: 5-Duct vs. 4-Duct Configurations

Figure 17 compares the results for DFI 5H vs. 4H configurations with RD and B50R50 fuels at the LN calibration. As was the case for Figure 15 and per the stated project objective of comparing to a petroleum-based ULSD, the baseline for comparison is once again the CDC 7H ULSD HN

calibration. Figure 17 shows that the 5H configuration yields larger PM and soot reductions than the 4H. Results for NO_x are mixed, with 5H giving a larger reduction for RD but smaller for B50R50. 5H tends to show higher emissions of HC, especially with B50R50 at M4 and M8 (see Figures A17 and A21). The BSEC penalty is nearly constant for the 5H and 4H configurations, suggesting that it is due at least in part to the timing retard and EGR addition required to achieve the measured NO_x reductions. Given the above, the DFI 5H configuration is deemed superior in general to the 4H.

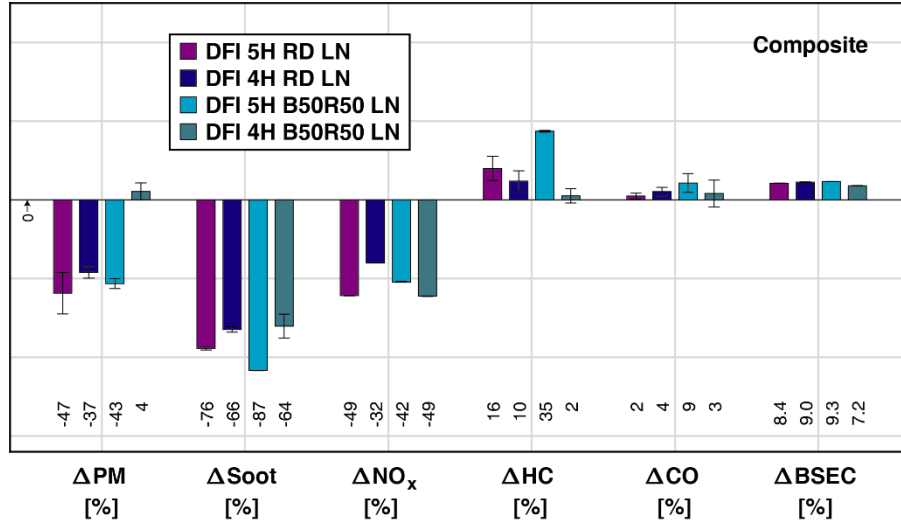


Figure 17. ISO 8178 composite results for DFI 4/5H RD and B50R50 LN calibrations. The baseline used for calculating changes is CDC 7H ULSD HN with the Tier 4 Final engine calibration.

Fuel Effects for DFI 4H Configuration

Though not a primary focus of discussion thus far, extensive DoE and ISO 8178 data were acquired for the DFI 4H configuration using ULSD, RD, B50R50, and B100 fuels. Figure 18 provides the composite ISO 8178 results from this testing. As was the case for Figures 15 and 17, the baseline for comparison is the CDC 7H ULSD HN calibration.

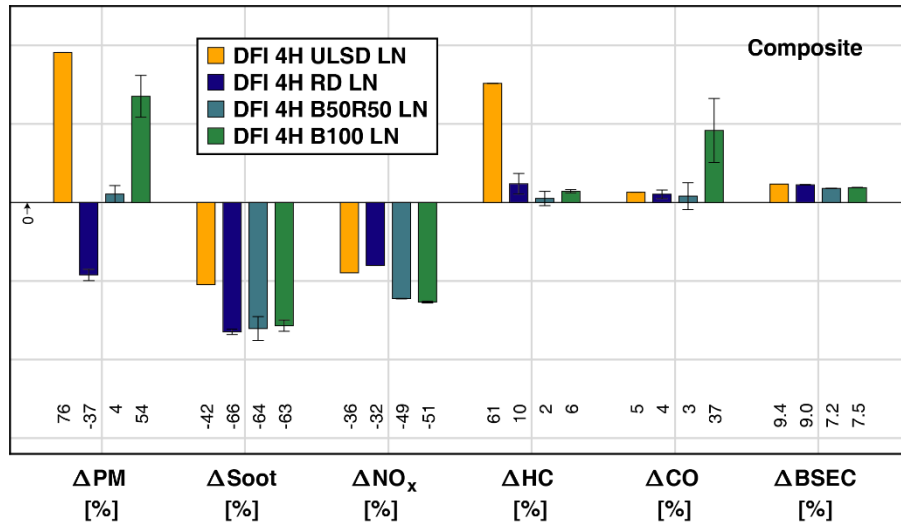


Figure 18. ISO 8178 composite results for DFI 4H LN calibrations with all test fuels. The baseline used for calculating changes is CDC 7H ULSD HN with the Tier 4 Final engine calibration.

Figure 18 shows that ULSD gives the highest PM, soot, and HC emissions, the second-highest NO_x emissions, and the largest BSEC penalty. Whereas ULSD gives 42% lower DFI soot emissions, the LLFCs yield ~65% soot reductions with DFI. Interestingly, B100 gives the second-highest PM emissions, despite it being an oxygenated fuel that is free of aromatics. PM increases roughly linearly with increasing biodiesel content from RD to B50R50 to B100. The lower volatility of biodiesel [24] may play a role in its higher PM levels. Nevertheless, the soot reduction for B100 is nearly as large as those for RD and B50R50, its NO_x reduction is slightly larger, and it has the second-lowest BSEC penalty of the fuels tested in the DFI 4H configuration. Given the DFI 4H performance data, B50R50 appears to provide the best balance of benefits.

Duct-Module Deposits

At the beginning of the test campaign, after the brand-new engine had been broken in by running CDC and acquiring baseline data with ULSD fuel for ~150 h, the cylinder head was swapped to one with a 4H DFI configuration. DoE testing of 4H DFI commenced in the order M7 → M2 → M3 → M6 → M1 → M5 → M8. After ~15 h of DFI testing and almost immediately after beginning testing at M8, HC emissions rose rapidly, and IMEP_g dropped substantially on Cylinder 4 and to a lesser extent on Cylinder 6. The cylinder head was removed, and the ducts in Cylinder 4 were found to be nearly completely obstructed with deposits. The Cylinder 6 ducts were in a less-severe condition with a partial obstruction visible within only one of the ducts. The duct modules in the rest of the cylinders were visually clean and unobstructed.

Given that the deposit issue was largely localized to Cylinder 4, the injector in that cylinder was replaced, with the original injector sent to the manufacturer for analysis. Also, the ULSD fuel and all fuels tested subsequently were treated with John Deere Fuel-Protect Keep Clean additive at a treat rate of 1500 ppm.

The analysis conducted by the injector manufacturer indicated that the exits of two of the four orifices on the injector that was removed from Cylinder 4 showed evidence of mechanical deformation. This injector was tested using a spray-visualization facility, and the sprays emanating from the deformed orifices were found to have wider spreading angles than the undamaged orifices. The working hypothesis is that the wider spreading angles contributed to the deposit formation, but this has not been confirmed.

SUMMARY AND CONCLUSIONS

This work represents the first known implementation and testing of DFI in a multi-cylinder engine. The study employed a 6-cylinder, 9-liter, baseline engine compliant with Tier 4 Final (T4F) off-road emissions regulations when paired with an aftertreatment system (ATS). The engine modifications for DFI were minimal, and the combustion system was not optimized for DFI. Rather, the cylinder head and pistons were machined to accommodate two new parts per cylinder—a duct module and a flange bolt—while the rest of the engine was left effectively unchanged. Four-hole/duct (4H) and five-hole/duct (5H) DFI configurations were carefully aligned, with the alignment procedure being refined between the 4H and 5H testing. Three low-lifecycle-CO₂ fuels (LLCFs) were tested with the 4H configuration, namely renewable diesel (RD), neat soy biodiesel (B100), and a 50/50 blend of B100 with RD denoted B50R50, as well as a petroleum-based ultra-low-sulfur diesel (ULSD). Only RD and B50R50 were tested with the 5H configuration. Design-of-experiments (DoE) testing was conducted for each DFI + fuel combination, from which a set of operating parameters (injection timing, EGR level, injection pressure, air-fuel ratio) was selected for each mode of the ISO 8178-C1 eight-mode steady-state off-road test cycle. The goal was to achieve simultaneous ~70% reductions in engine-out soot and lifecycle-CO₂ emissions and ~50% reductions in engine-out NO_x, without a significant degradation in other emissions or brake-specific energy consumption (BSEC), relative to the baseline conventional diesel combustion (CDC) engine burning petroleum-derived ULSD. Following are some significant findings from the work:

1. DoE tests showed that DFI with LLCFs can provide significant benefits, with soot and NO_x reductions up to 98% and 77%, respectively, and brake-specific energy consumption (BSEC) changes from a 41% improvement to a 12% penalty.
2. Only light-load conditions showed BSEC improvements with DFI, but all operating conditions were selected to minimize soot and reduce NO_x by ~50% rather than to minimize BSEC.
3. DFI with LLCFs performed well over the composite ISO 8178 test cycle, with the 5H DFI configuration with B50R50 achieving 87% lower soot, 42% lower NO_x, relatively small increases in hydrocarbon (HC) and carbon-monoxide (CO) emissions, and a BSEC increase of 9.3% relative to the baseline of T4F 7H CDC with ULSD. For RD, the 5H DFI configuration

attained 76% lower soot, 49% lower NO_x, larger but still relatively small increases in HC and CO emissions, and a BSEC increase of 8.4%.

4. When 7H CDC was compared to 5H DFI using RD for both (to eliminate the fuel effect) and keeping the composite engine-out NO_x constant, DFI delivered a 69% soot reduction but a BSEC increase of 5.3%.
5. The 5H DFI configuration achieved larger soot and PM reductions than 4H DFI; hence, it was deemed superior, though it did lead to nominal increases in HC, CO, and BSEC.
6. While all three LLCFs enabled substantial reductions of soot, NO_x, and lifecycle-CO₂ emissions with 4H DFI over the test cycle, B50R50 is considered to offer the best balance of characteristics.
7. The duct module in one engine cylinder became plugged with deposits shortly after the commencement of 4H DFI testing with ULSD. The injector in that cylinder was replaced (and subsequently found to have deformations at the exits of two of its four orifices leading to wider sprays), all subsequent fuels were treated with a detergent additive, and no further serious plugging events were encountered.

Based on the above findings and the fact that this is the first multi-cylinder engine test of DFI, it is concluded that further research and development efforts are justified. In particular, optimization to minimize BSEC as well as engine-out emissions is a high priority, as is the further investigation of fuel effects on DFI performance, transient effects, and durability considerations.

Acronyms and Abbreviations

4/5/7H	four-/five-/seven-hole and/or duct injector configuration
ATDC	after top-dead-center
ATS	aftertreatment system
B100	neat soy biodiesel
B50R50	50/50 blend by volume of B100 and RD
BSEC	brake-specific energy consumption
CAD	crank-angle degrees
CDC	conventional diesel combustion
CO	carbon monoxide
CO ₂	carbon dioxide
D	duct diameter
DEF	diesel exhaust fluid
DFI	ducted fuel injection
DoE	design of experiments
DPF	diesel particulate filter
EGR	exhaust-gas recirculation
G	“gap” (i.e., standoff distance) from injector orifice exit to duct inlet

HC	hydrocarbon
HN	high-NO _x calibration
IMEP _g	gross indicated mean effective pressure
ISO	International Organization for Standardization
L	duct length
LLCF	low-lifecycle-CO ₂ fuel
LN	low-NO _x calibration
M1-8	Mode 1 – Mode 8 of the ISO 8178 test cycle
NO _x	nitrogen oxides
PM	particulate matter
RD	renewable diesel
SCR	selective catalytic reduction
SOI	start of injection
T4F	Tier 4 Final emissions regulations
ULSD	ultra-low-sulfur diesel
σ	standard deviation

Acknowledgments

The project team is grateful to the U.S. Department of Energy (DOE) Vehicle Technologies Office and Office of Technology Transitions for their co-sponsorship of this research. The authors also thank the organizations and representatives participating in Coordinating Research Council Project AVFL-44, contractor Brian Bratvold, and intern Sebastian Barboza. This article has been authored by an employee of National Technology & Engineering Solutions of Sandia, LLC, under Contract No. DE-NA0003525 with DOE. The employee owns all right, title, and interest in and to the article and is solely responsible for its contents. The United States Government retains and the publisher, by accepting the article for publication, acknowledges that the United States Government retains a non-exclusive, paid-up, irrevocable, world-wide license to publish or reproduce the published form of this article or allow others to do so, for United States Government purposes. The DOE will provide public access to these results of federally sponsored research in accordance with the DOE Public Access Plan <https://www.energy.gov/downloads/doe-public-access-plan>. This paper describes objective technical results and analysis. Any subjective views or opinions that might be expressed in the paper do not necessarily represent the views of the DOE or the United States Government.

APPENDIX

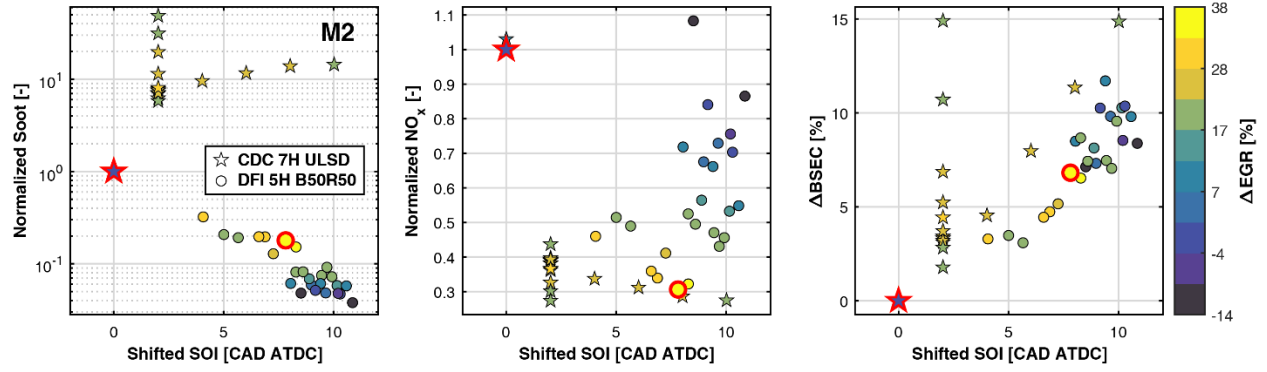


Figure A1. DoE data showing normalized engine-out soot and NO_x as well as ΔBSEC vs. shifted SOI timing and relative change in EGR level for CDC 7H ULSD vs. DFI 5H B50R50 at M2 (100% speed, 75% load) of the ISO 8178 test cycle.

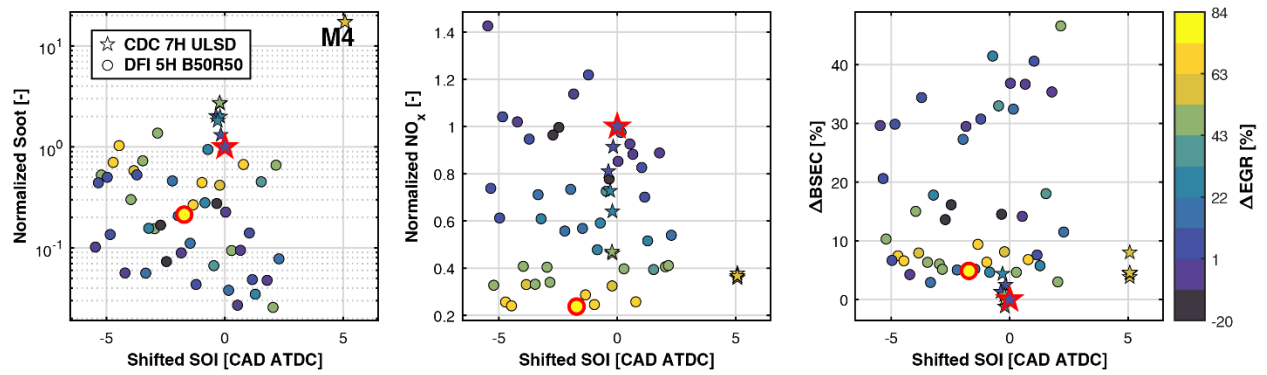


Figure A2. DoE data showing normalized engine-out soot and NO_x as well as ΔBSEC vs. shifted SOI timing and relative change in EGR level for CDC 7H ULSD vs. DFI 5H B50R50 at M4 (100% speed, 10% load) of the ISO 8178 test cycle.

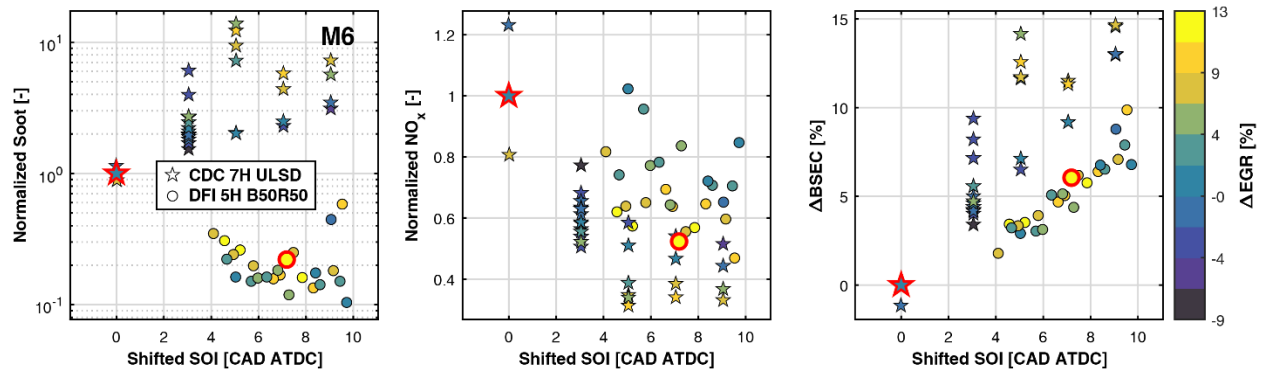


Figure A3. DoE data showing normalized engine-out soot and NO_x as well as ΔBSEC vs. shifted SOI timing and relative change in EGR level for CDC 7H ULSD vs. DFI 5H B50R50 at M6 (75% speed, 75% load) of the ISO 8178 test cycle.

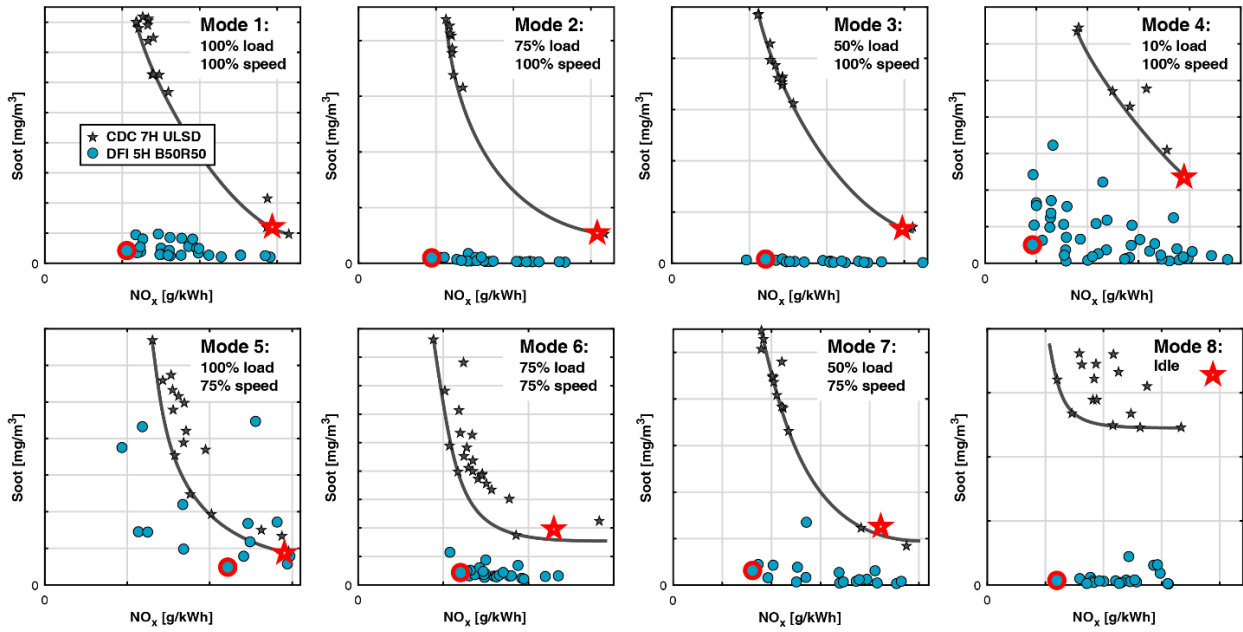


Figure A4. Engine-out soot/NO_x tradeoff plots from DoE data for CDC 7H ULSD and DFI 5H B50R50 for all modes of the ISO 8178 test cycle. Substantial emissions benefits are possible with DFI and B50R50.

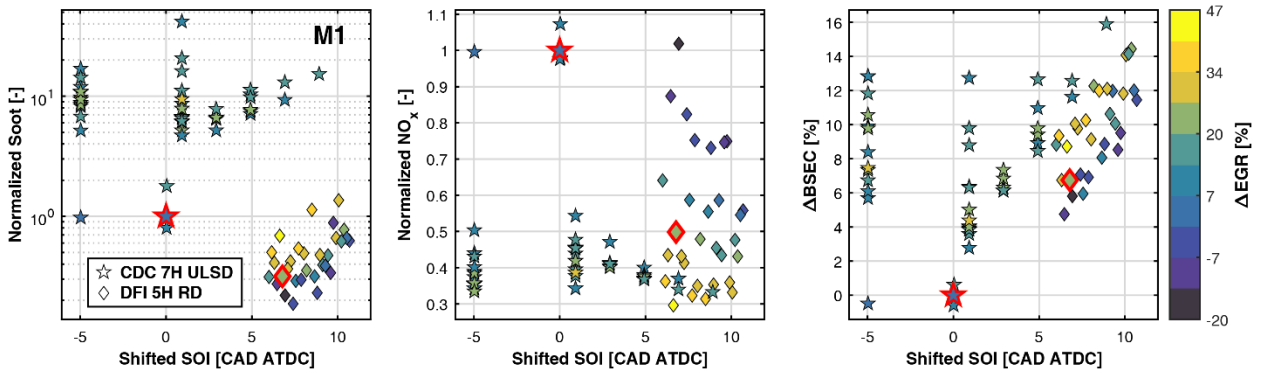


Figure A5. DoE data showing normalized engine-out soot and NO_x as well as Δ BSEC vs. shifted SOI timing and relative change in EGR level for CDC 7H ULSD vs. DFI 5H RD at M1 (100% speed, 100% load) of the ISO 8178 test cycle.

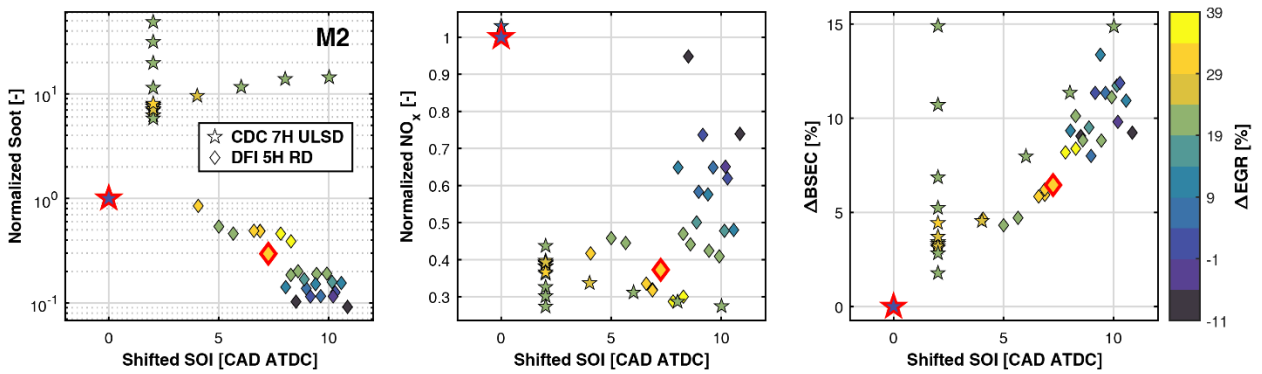


Figure A6. DoE data showing normalized engine-out soot and NO_x as well as Δ BSEC vs. shifted SOI timing and relative change in EGR level for CDC 7H ULSD vs. DFI 5H RD at M2 (100% speed, 75% load) of the ISO 8178 test cycle.

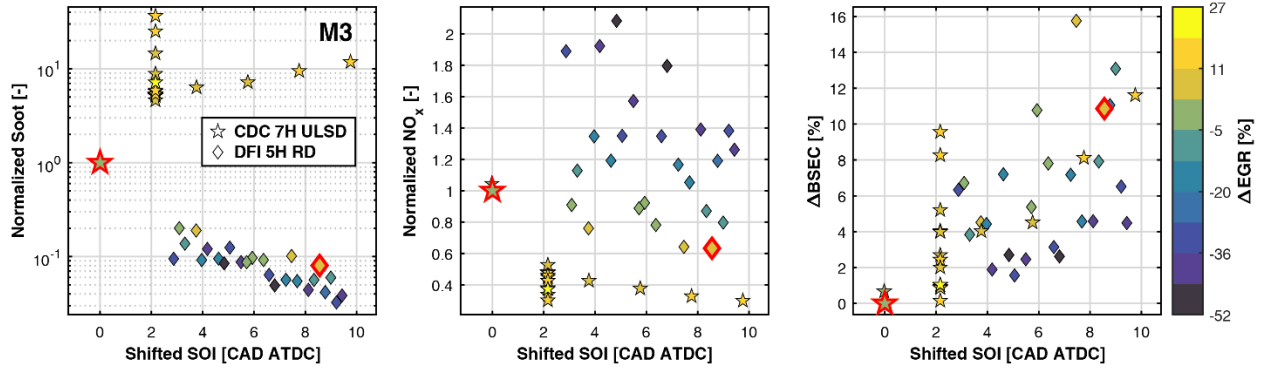


Figure A7. DoE data showing normalized engine-out soot and NO_x as well as ΔBSEC vs. shifted SOI timing and relative change in EGR level for CDC 7H ULSD vs. DFI 5H RD at M3 (100% speed, 50% load) of the ISO 8178 test cycle.

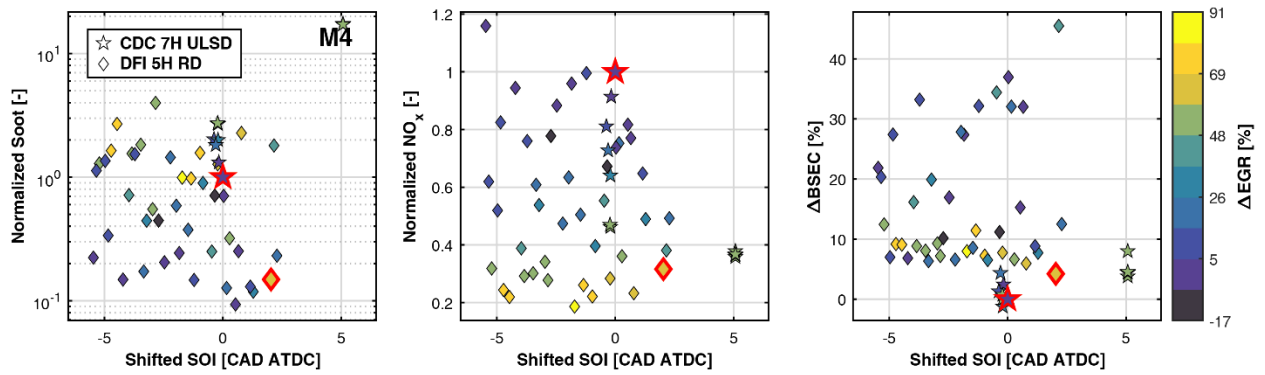


Figure A8. DoE data showing normalized engine-out soot and NO_x as well as ΔBSEC vs. shifted SOI timing and relative change in EGR level for CDC 7H ULSD vs. DFI 5H RD at M4 (100% speed, 10% load) of the ISO 8178 test cycle.

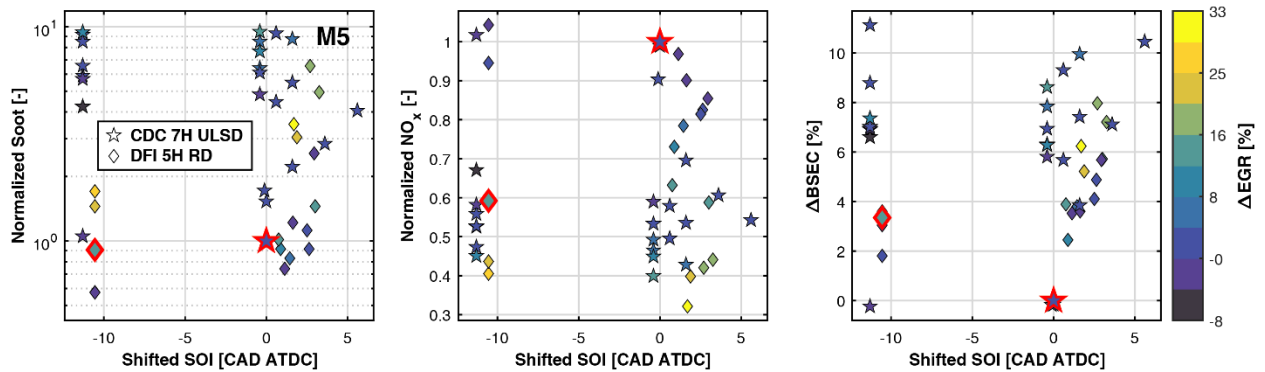


Figure A9. DoE data showing normalized engine-out soot and NO_x as well as ΔBSEC vs. shifted SOI timing and relative change in EGR level for CDC 7H ULSD vs. DFI 5H RD at M5 (75% speed, 100% load) of the ISO 8178 test cycle.

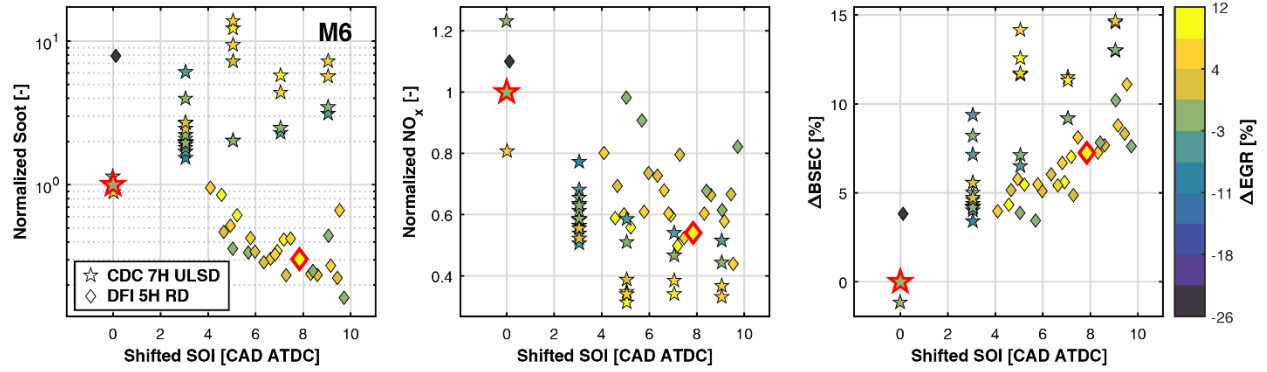


Figure A10. DoE data showing normalized engine-out soot and NO_x as well as ΔBSEC vs. shifted SOI timing and relative change in EGR level for CDC 7H ULSD vs. DFI 5H RD at M6 (75% speed, 75% load) of the ISO 8178 test cycle.

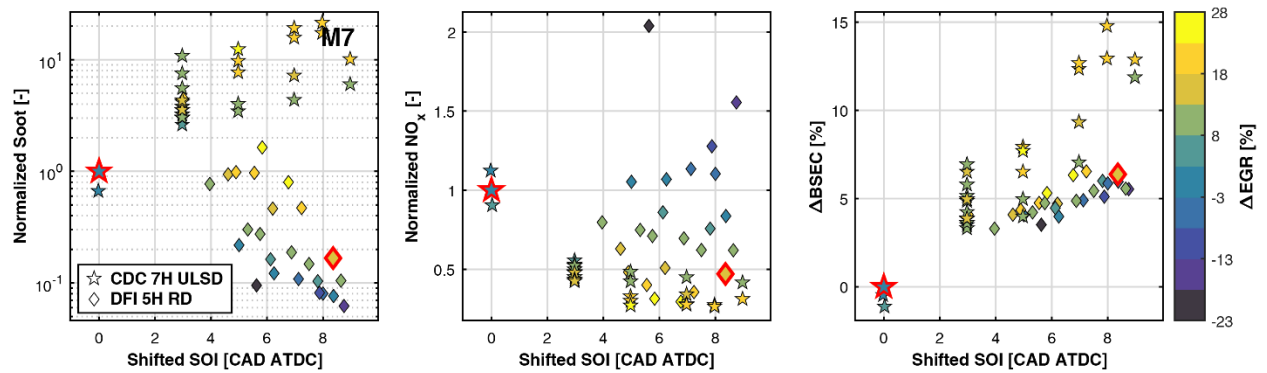


Figure A11. DoE data showing normalized engine-out soot and NO_x as well as ΔBSEC vs. shifted SOI timing and relative change in EGR level for CDC 7H ULSD vs. DFI 5H RD at M7 (75% speed, 50% load) of the ISO 8178 test cycle.

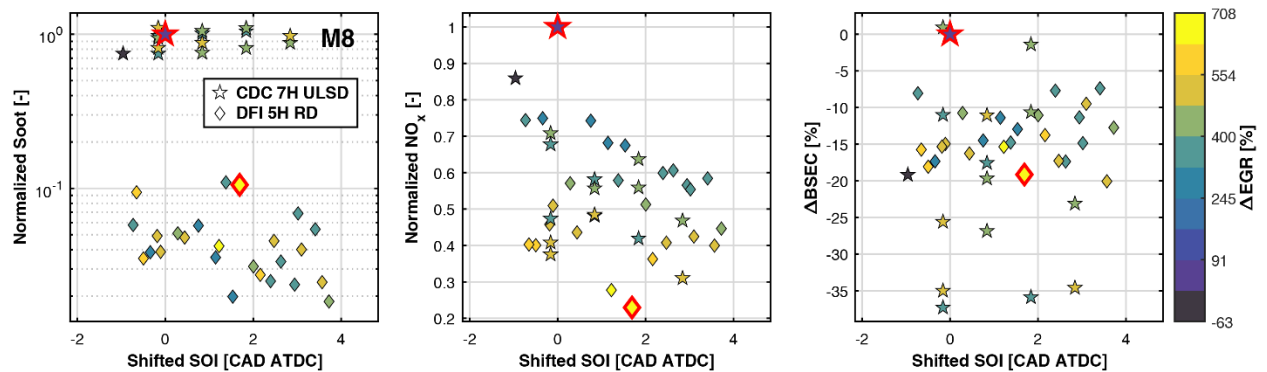


Figure A12. DoE data showing normalized engine-out soot and NO_x as well as ΔBSEC vs. shifted SOI timing and relative change in EGR level for CDC 7H ULSD vs. DFI 5H RD at M8 (idle) of the ISO 8178 test cycle.

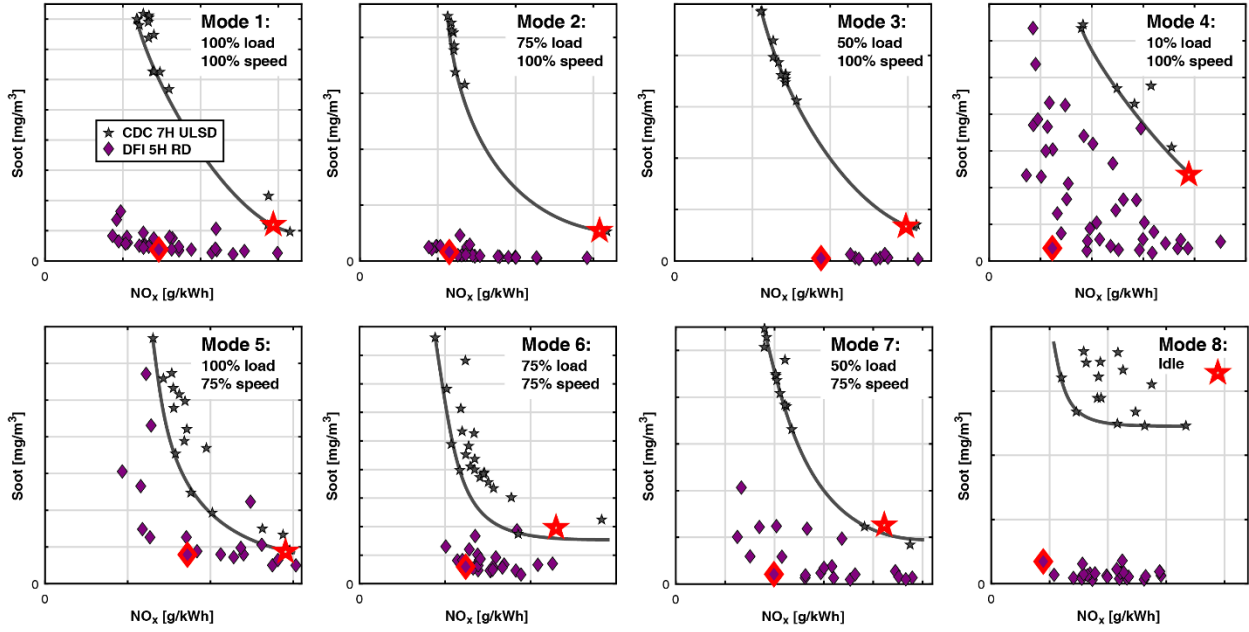


Figure A13. Engine-out soot/NOx tradeoff plots from DoE data for CDC 7H ULSD and DFI 5H RD for all modes of the ISO 8178 test cycle. Substantial emissions benefits are possible with DFI and RD.

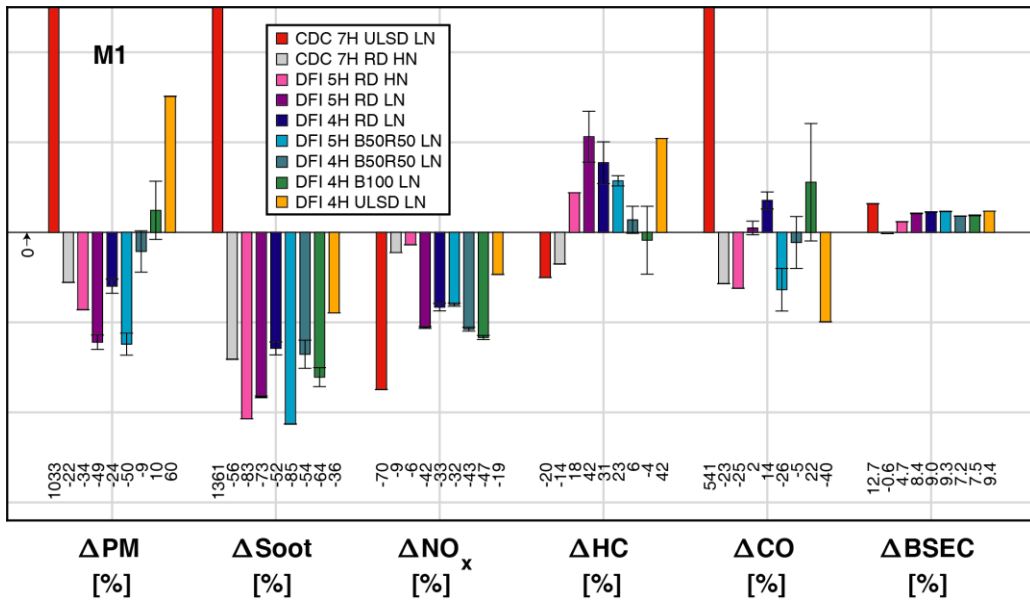


Figure A14. ISO 8178 data showing changes relative to CDC 7H ULSD HN at M1.

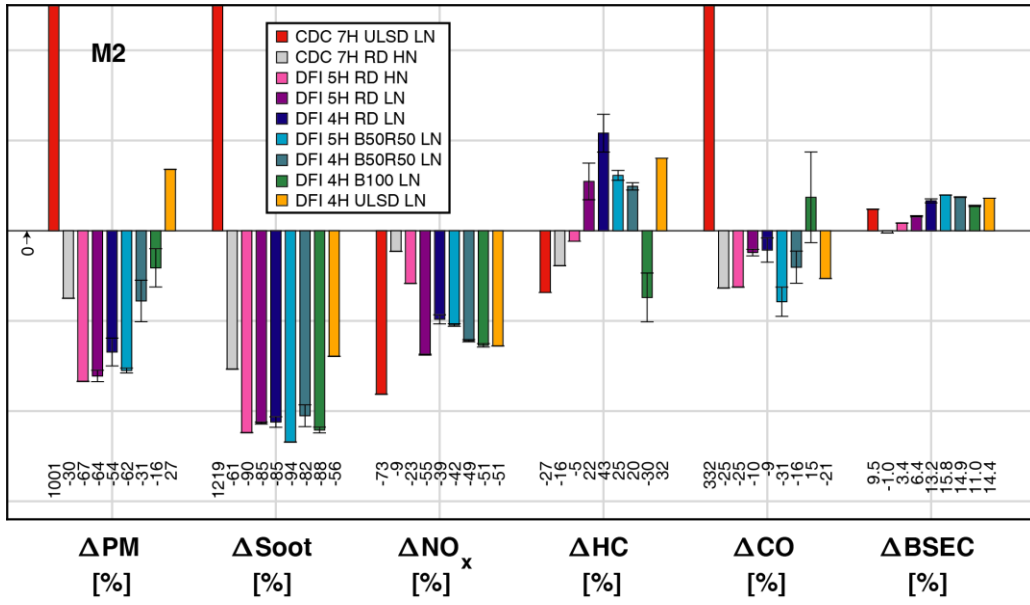


Figure A15. ISO 8178 data showing changes relative to CDC 7H ULSD HN at M2.

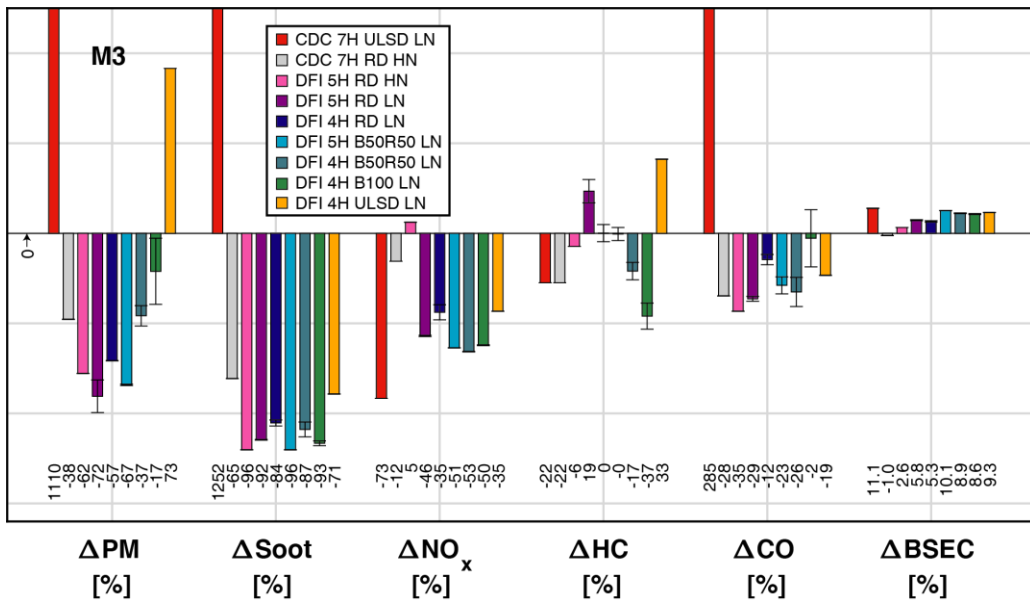


Figure A16. ISO 8178 data showing changes relative to CDC 7H ULSD HN at M3.

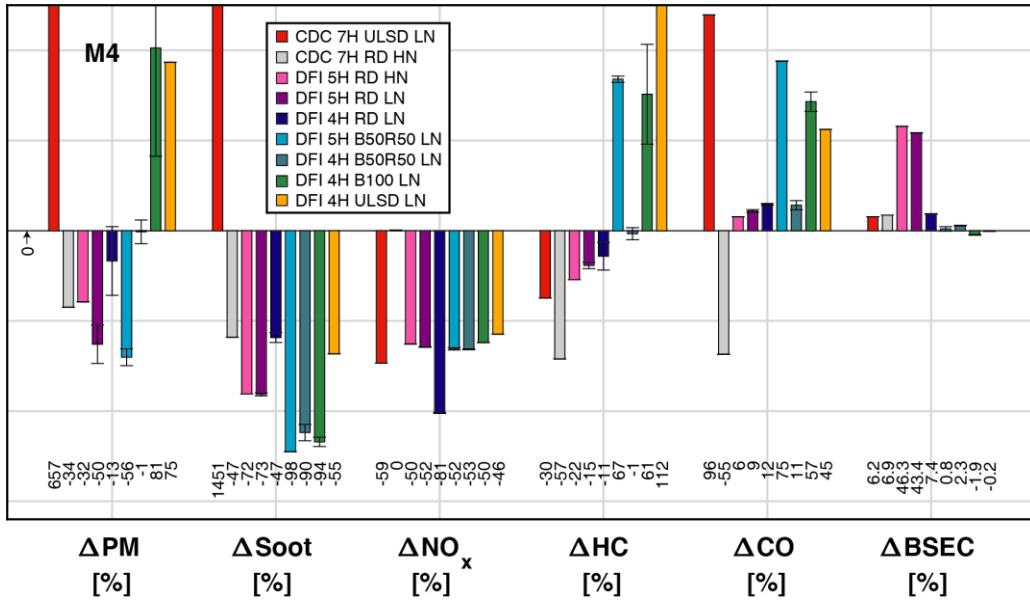


Figure A17. ISO 8178 data showing changes relative to CDC 7H ULSD HN at M4.

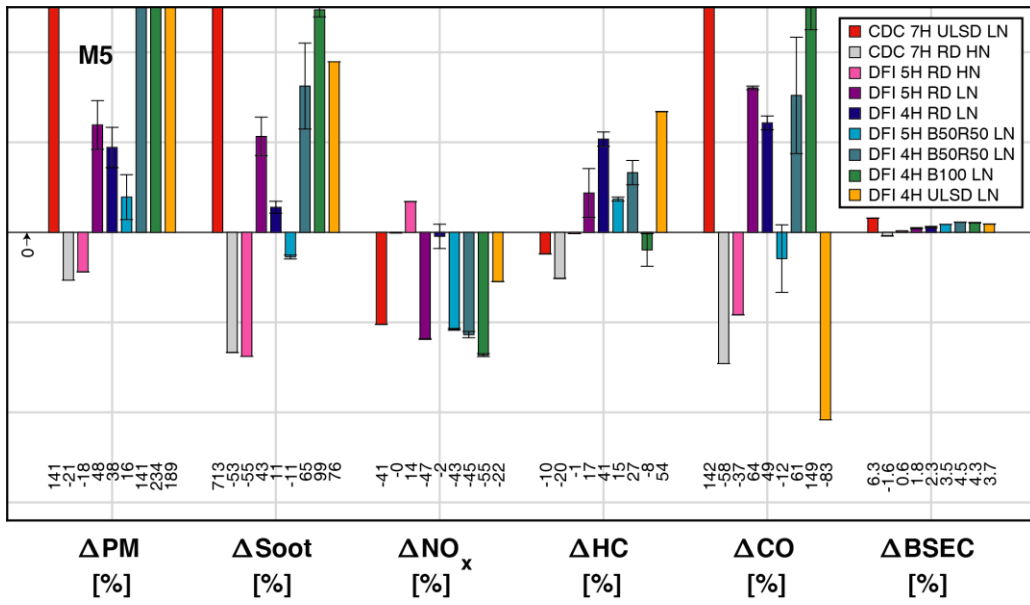


Figure A18. ISO 8178 data showing changes relative to CDC 7H ULSD HN at M5.

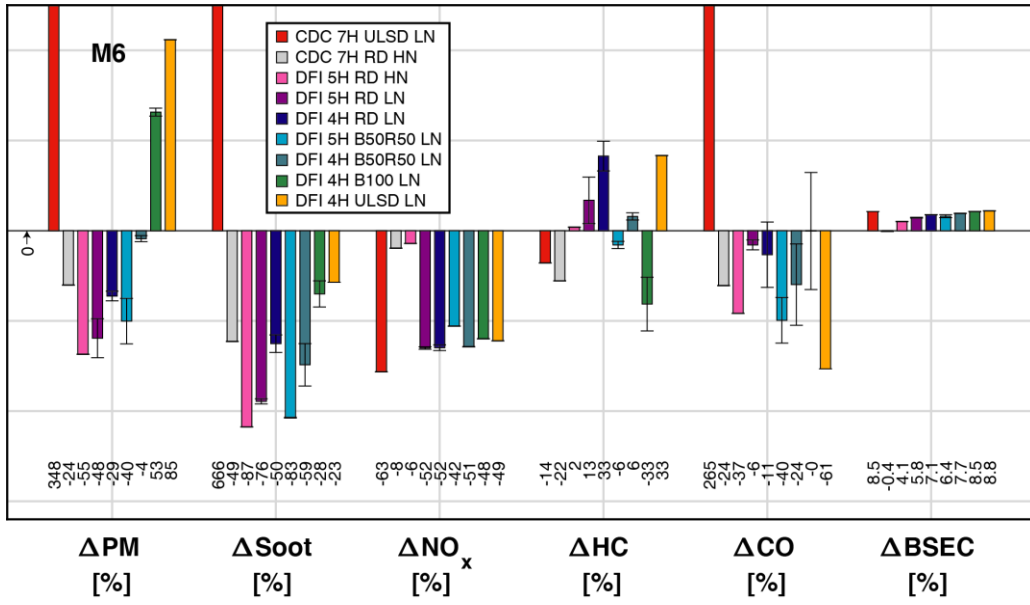


Figure A19. ISO 8178 data showing changes relative to CDC 7H ULSD HN at M6.

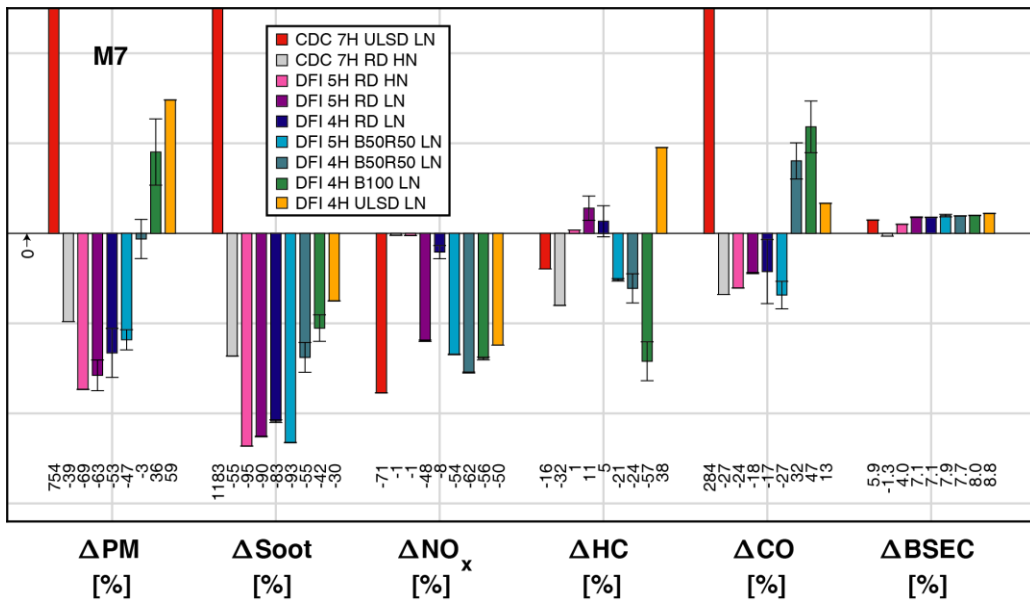


Figure A20. ISO 8178 data showing changes relative to CDC 7H ULSD HN at M7.

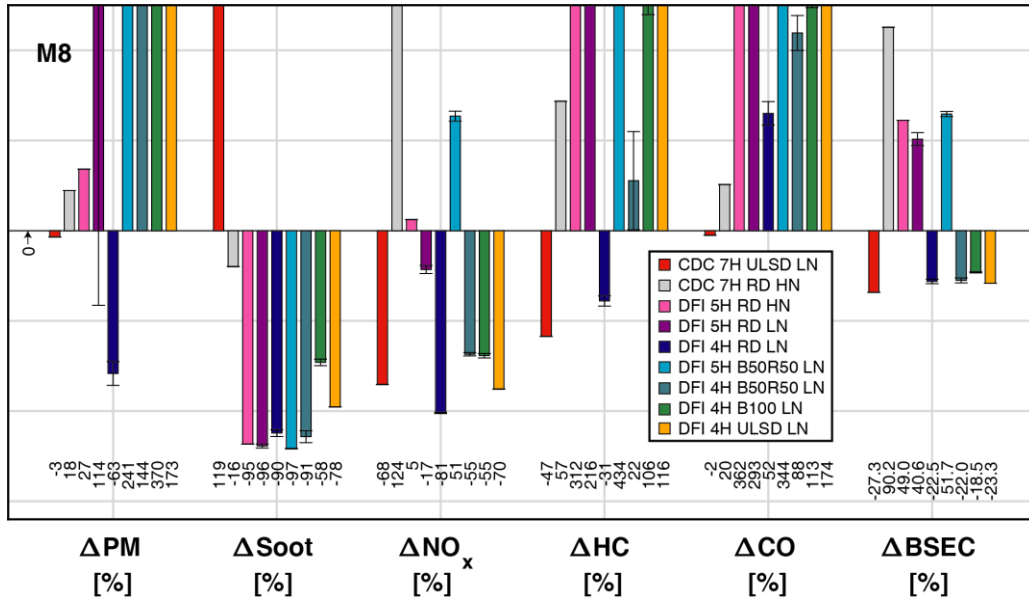


Figure A21. ISO 8178 data showing changes relative to CDC 7H ULSD HN at M8.

References

- ExxonMobil, "Energy Demand Trends," Aug. 26, 2024. Online source, <https://corporate.exxonmobil.com/sustainability-and-reports/global-outlook/energy-demand-trends>. Accessed Feb. 24, 2025.
- Praveena, V. and Martin, M.L.J., "A Review on Various after Treatment Techniques to Reduce NO_x Emissions in a CI Engine," *Journal of the Energy Institute* **91**(5):704-720, 2018, doi:10.1016/j.joei.2017.05.010.
- Mueller, C.J., Nilsen, C.W., Ruth, D.J., Gehmlich, R.K., Pickett, L.M., and Skeen, S.A., "Ducted Fuel Injection: A New Approach for Lowering Soot Emissions from Direct-Injection Engines," *Applied Energy* **204**:206-220, 2017, doi:10.1016/j.apenergy.2017.07.001.
- Millo, F., Piano, A., Peiretti Paradisi, B., Postriotti, L., Pieracci, L., Bianco, A., Pesce, F.C., and Vassallo, A., "Ducted Fuel Injection: Experimental and Numerical Investigation on Fuel Spray Characteristics, Air/Fuel Mixing and Soot Mitigation Potential," *Fuel* **289**:119835, 2021, doi:10.1016/j.fuel.2020.119835.
- Godbold, C., Gupta, I., Kurtz, E., Mueller, C.J., Genzale, C., and Steinberg, A., "Experimental Investigation of Mixing Phenomena for Ducted Fuel Injection," *Proceedings of the Combustion Institute* **40**(1):105385, 2024, doi:10.1016/j.proci.2024.105385.
- Guo, J., Brouzet, D., Chung, W.T., and Ihme, M., "Analysis of Ducted Fuel Injection at High-Pressure Transcritical Conditions Using Large-Eddy Simulations," *International Journal of Engine Research* **25**(2):305-319, 2024, doi:10.1177/14680874231170659.
- Gehmlich, R.K., Mueller, C.J., Ruth, D.J., Nilsen, C.W., Skeen, S.A., and Manin, J., "Using Ducted Fuel Injection to Attenuate or Prevent Soot Formation in Mixing-Controlled Combustion Strategies for Engine Applications," *Applied Energy* **226**:1169-1186, 2018, doi:10.1016/j.apenergy.2018.05.078.
- Millo, F., Segatori, C., Piano, A., Peiretti Paradisi, B., and Bianco, A., "An Engine Parameters Sensitivity Analysis on Ducted Fuel Injection in Constant-Volume Vessel Using Numerical Modeling." SAE International. 2021.
- Nilsen, C.W., Biles, D.E., Wilmer, B.M., and Mueller, C.J., "Investigating the Effects of Duct Length and Diameter and Fuel Injector Orifice Diameter in a Compression-Ignition Engine Equipped with Ducted Fuel Injection," *Applications in Energy and Combustion Science*, 2021, doi:10.1016/j.jaecs.2021.100030.
- Svensson, K., Fitzgerald, R., and Martin, G., "Ducted Fuel Injection: An Experimental Study on Optimal Duct Size." SAE International. 2022.
- Şener, R., Nyrenstedt, G., Baumgard, K.J., and Mueller, C.J., "Determining Tolerance Requirements for Spray-Duct Alignment in Ducted Fuel Injection", 2024.

12. Svensson, K., Kim, C., Seiler, P., Martin, G., and Koci, C., "Performance and Emission Results from a Heavy-Duty Diesel Engine with Ducted Fuel Injection." SAE International. 2021.
13. Piano, A., Segatori, C., Millo, F., Pesce, F.C., and Vassallo, A.L., "Investigation of Ducted Fuel Injection Implementation in a Retrofitted Light-Duty Diesel Engine through Numerical Simulation," *SAE International Journal of Engines* **16**(5):643-661, 2023, doi:10.4271/03-16-05-0038.
14. Pastor, J.V., Micó, C., Lewiski, F., and Bin-Khalid, U., "Evaluation of the Ducted Fuel Injection Concept for Medium Duty Engines and Multi-Hole Nozzles: An Optical Analysis," *Applied Energy* **376**, 2024, doi:10.1016/j.apenergy.2024.124305.
15. Lehtoranta, K., Matilainen, P., Åsenbrygg, J.M., Lievonen, A., Kinnunen, T.J.J., Keskinen, J., and Solla, A., "Particle Oxidation Catalyst in Light Duty and Heavy Duty Diesel Applications," 2007, doi:10.4271/2007-24-0093.
16. Fredholm, S., Andersson, S., Marsh, P., D'Aniello, M.J., Zammit, M.G., and Brear, F., "Development of Diesel Oxidation Catalysts for Heavy Duty Engines," 1993, doi:10.4271/932719.
17. Ogura, Y., Kibe, K., Kaneko, S., Ito, Y., and Aono, N., "Development of Oxidation Catalyst for Diesel Engine," 1994, doi:10.4271/940240.
18. Narusawa, K., Hori, S., Sato, T., and Abe, T., "The Evaluation of Oxidation Catalysts for Diesel Trucks," 1995, doi:10.4271/950157.
19. Ladommatos, N., Xiao, Z., and Zhao, H., "Effects of Fuels with a Low Aromatic Content on Diesel Engine Exhaust Emissions," *Proceedings of the Institution of Mechanical Engineers, Part D: Journal of Automobile Engineering* **214**(7):779-794, 2000, doi:10.1243/0954407001527646.
20. Pitz, W.J. and Mueller, C.J., "Recent Progress in the Development of Diesel Surrogate Fuels," *Progress in Energy and Combustion Science* **37**(3):330-350, 2011, doi:10.1016/j.pecs.2010.06.004.
21. Buurman, N.J., Nyrenstedt, G., and Mueller, C.J., "Ducted Fuel Injection Provides Consistently Lower Soot Emissions in Sweep to Full-Load Conditions," *SAE International Journal of Engines* **17**(1), 2023, doi:10.4271/03-17-01-0001.
22. Nyrenstedt, G., Nilsen, C.W., Biles, D.E., and Mueller, C.J., "Ducted Fuel Injection with Low-Net-Carbon Fuels as a Solution for Meeting Future Emissions Regulations," *Fuel* **338**:127167, 2023, doi:10.1016/j.fuel.2022.127167.
23. Mueller, C.J., Nilsen, C.W., Biles, D.E., and Yraguen, B.F., "Effects of Fuel Oxygenation and Ducted Fuel Injection on the Performance of a Mixing-Controlled Compression-Ignition Optical Engine with a Two-Orifice Fuel Injector," *Applications in Energy and Combustion Science*, 2021, doi:10.1016/j.jaecs.2021.100024.
24. The Biodiesel Handbook, Ed. by Knothe, G., Krahl, J., and Van Gerpen, J. AOCS Press, Champaign, IL, 2010.